The chemistry of fine-grained terrigenous sediments reveals a chemically evolved Paleoarchean emerged crust

Nicolas D. Greber[1,*], Nicolas Dauphas[2]

[1] *Département des sciences de la Terre, Université de Genève, 1205, Genève, Switzerland*

[2] *Origins Laboratory, Department of the Geophysical Sciences and Enrico Fermi Institute, The University of Chicago, Chicago, IL 60615, USA*

To be submitted to:

Geochimica et Cosmochimica Acta

*Corresponding author. E-mail: nicolas.greber@unige.ch

Abstract

The nature of the rocks exposed to weathering and erosion on continents exerts an important control on weathering feedbacks and the supply of nutrients to the oceans. It also reflects the prevailing tectonic regime responsible for the formation of continents. How the chemical and lithological compositions of the continents evolved through time is, however, still a matter of debate. We use an extensive compilation of terrigenous sediment compositions to better constrain the nature of rocks at the surface of continents at 3.25 Gyr ago and 250 Myr ago. Specifically, we use geochemical ratios that are sensitive indicators of komatiite, mafic, and felsic rocks in the provenance of the sediments. Our results show that the average Al_2O_3/TiO_2 ratio of fine-grained terrigenous sediments decreased slightly over time from 26.2 ± 1.3 in the Archean to 22.1 ± 1.1 (2SE) in the Phanerozoic. In contrast, in the same time interval, the average Zr/TiO_2 ratio stayed nearly constant at ~245 throughout Earth's history. Considering the distinct behavior of Al, Ti and Zr during sedimentary processes, we find that hydrodynamic mineral sorting had a minor effect on the chemical composition of Archean fine-grained sediments, but could have been more effective during periods of supercontinents. We show that the compositions of Phanerozoic sediments (Al_2O_3/TiO_2, Zr/TiO2, La/Sc, Th/Sc, Ni/Co, Cr/Sc) are best explained with igneous rocks at the surface of continents consisting of 76 ± 8 wt% felsic, 14 ± 6 wt% Arc-basalts and 10 ± 2 wt% within-plate basalts, most likely in the form of continental flood basalts. Applying the same mass-balance calculations to the Paleoarchean suggests continental landmasses with 65 ± 7 wt% felsic, 25 ± 6 wt% mafic and 11 ± 3 wt% ultramafic rocks (all 2SE), likely in the form of komatiites. The presence of volumetrically abundant felsic rocks at the surface of continents (as evident from the sediment record) as well as at mid-crustal levels (as evident from presently exposed igneous rock record) in Paleoarchean cratons is currently best explained with the onset of subduction magmatism before 3.25 Ga.

1 Introduction

In recent years, growing interest has been paid to the connections between Earth's mantle, the continental crust, and near surface environments. Fine-grained terrigenous sediments are key geological witnesses of how these reservoirs evolved through time. For example, the chemical and isotopic compositions of detrital sediments can be used to quantify the redox state of the atmosphere and oceans through time (e.g. Canfield, 2005; Lyons *et al.,* 2014, and references therein) as well as the composition of the continental crust that was subjected to weathering and erosion (hereafter called "emerged crust") (Condie, 1993; Rudnick and Gao, 2003; Taylor and McLennan, 1985). Such studies have helped identify temporal and possibly causal relationships between shifts in the composition and extent of the continental crust with dramatic changes in surface environments and habitats for life, such as the Great Oxidation Event (GOE) (Bindeman *et al.*, 2016; 2018; Condie, 2005; Greber *et al.*, 2017a; Smit and Mezger, 2017).

The goal of our study is to reconstruct the rock composition of the emerged crust by using the chemical compositions of sediments. This task is challenging, as processes such as chemical weathering, diagenesis and hydrodynamic sorting of minerals can bias the chemical and isotopic compositions of sediments compared to those of their source rocks. In particular, elements that have high solubilities in water like Mg, Ca, Sr, K and Na can be fractionated during weathering and sedimentary processes (Taylor and McLennan, 1985). Thus, one often relies on ratios of elements that are mostly insoluble, and use these to estimate the bulk composition of the emerged crust. Examples of element ratios that were used for this purpose are La/Sc, Th/Sc, Th/Co, Ni/Co, Cr/Zn, Th/Cr, La/Cr and Cr/U (Condie, 1993; Large *et al.*, 2018; Smit and Mezger, 2017; Tang *et al.*, 2016; Taylor and McLennan, 1985). The observed shifts in the element ratios involving either Ni or Cr of fine-grained terrigenous sediments towards the Archean-Proterozoic boundary were used to argue for a largely mafic emerged crust prior to 3.0 Gyr, which would have changed to be dominated

by felsic rocks by around 2.5 Gyr (Large *et al.*, 2018; Tang *et al.*, 2016). This change in the nature of the continental crust was used to argue for the initiation of modern style plate tectonics at ~3.0 Gyr ago (Dhuime *et al.*, 2015; Tang *et al.*, 2016). It was also suggested that the fast transition from mafic to felsic rocks could have caused the first irreversible rise in atmospheric oxygen that occurred at around 2.5 Gyr ago (Lee *et al.*, 2016; Smit and Mezger, 2017). However, this interpretation of the chemical composition of fine-grained terrigenous sediments was recently questioned based on the Ti isotopic composition of old sediments. As the Ti isotopic composition of common igneous rocks correlates with the degree of magmatic differentiation (Greber *et al.*, 2017b; Millet and Dauphas, 2014; Millet *et al.*, 2016; Deng *et al.*, 2019), the Ti isotopic signature of fine-grained terrigenous sediments can be used as a proxy to reconstruct the chemical composition of the emerged crust (Greber *et al.*, 2017a). In contrast to the proxies that rely on element ratios, no major change in the Ti isotopic composition of the sediments was found since ~3.5 Gyr ago, implying that the emerged crust contained >50 wt% felsic lithologies since then (Greber *et al.*, 2017a). A potential explanation for the inconsistencies between the different studies is that Ni and Cr concentrations in sediments are not tracking the amount of exposed mafic crust, but record instead the greater contribution of komatiites and ultramafic rocks in the Archean compared to the Proterozoic and Phanerozoic (Greber *et al.*, 2017a). Deng et al. (2019) argued instead that the heavy Ti isotopic composition of Archean terrigenous sediments might be consistent with an emerged crust made primarily of plume-related tholeiitic basalts and differentiated rocks akin to those found today in Hawaii or Iceland. Further work is also needed to assess whether Ti isotope systematics can be affected by hydrodynamic grain size sorting and weathering.

To evaluate the reasons for the observed discrepancies between the different studies, we compiled Al, Ti and Zr concentrations in fine-grained terrigenous sediments from the literature and use already published compilations of Cr, Ni, Co, Sc, Th and La concentrations of sediments (Greber

95 *et al.*, 2017a; Tang *et al.*, 2016; Taylor and McLennan, 1985) to reconstruct the lithological com-
96 position of the emerged continents 3.25 Gyr ago, a time of contention with regard to the nature of
97 the emerged crust and for which a large enough database of fine-grained terrigenous sediments is
98 available to draw meaningful conclusions.

99

100 **2 Proxy ratios and mineral sorting in sediments**

101 An element used to evaluate the provenance of fine-grained terrigenous sediments should ide-
102 ally fulfill the following criteria: (*i*) it should be fluid immobile and thus immune to processes
103 involving fluid-rock interaction, (*ii*) it should not be involved in biological processes, (*iii*) its con-
104 centration should be distinct among the different lithologies in the provenance, and (*iv*) it should
105 be minimally affected by mineral sorting during sedimentary processes. Aluminum, Ti and Zr are
106 among the most fluid immobile elements known (Taylor and McLennan, 1985) and are unim-
107 portant in biological processes. They thus fulfill criteria (*i*) and (*ii*). Because Ti is overall more
108 compatible during fractional crystallization than both Zr and Al, the Al_2O_3/TiO_2 and the Zr/TiO_2
109 ratios in igneous rocks correlate positively with the SiO_2 concentration, which is used here as proxy
110 for the magmatic evolution of an igneous system (Fig. 1). Also, no major difference can be ob-
111 served in these geochemical trends between rocks of Archean and post-Archean age as well as
112 between samples belonging to the alkaline, tholeiitic and calc-alkaline magmatic series (Fig.1 and
113 supplementary Fig. S1). Thus, the Al_2O_3/TiO_2 and Zr/TiO_2 ratios can be used to discriminate be-
114 tween felsic ($63 < SiO_2 < 80$ wt%) and mafic components ($45 < SiO_2 < 52$ wt%; $MgO < 18$ wt%).
115 These elements thus fulfill criterion (*iii*). Regarding criterion (*iv*), Garcia et al. (1994) suggested
116 that Al and Ti behaved similarly during sediment transport and that their ratio should not be af-
117 fected by mineral sorting, allowing one to use the Al_2O_3/TiO_2 ratio in fine-grained terrigenous
118 sediments to evaluate the chemical and lithological composition of their provenance (Hayashi *et*

119 *al.*, 1997). Although published studies indicate that these two elements do not get strongly decou-
120 pled during sedimentary processes, Al is mainly hosted in clay minerals, while Ti is also partly
121 concentrated in resistant heavy minerals such as ilmenite or rutile. Thus, more work is needed to
122 ascertain that the Al_2O_3/TiO_2 ratio is not fractionated by mineral sorting. Zirconium can be frac-
123 tionated during sedimentary transport due to the preferential sorting of zircon grains into sand-
124 stones (Garcia *et al.*, 1991; 1994; Garçon *et al.*, 2013b; 2014) and the Zr/TiO_2 ratio of fine-grained
125 terrigenous sediments might be affected by mineral sorting during riverine transport and sedimen-
126 tation. The extent to which Al, Ti and Zr concentrations can be fractionated by mineral sorting
127 processes is currently difficult to quantify and depends on several factors; most importantly the
128 chemical and mineralogical composition of the provenance, the fluvial transport distance, and the
129 fluid motion pattern (Bouchez *et al.*, 2011; Garçon *et al.*, 2013a). However, it is reasonable to
130 assume that if any bias associated with mineral sorting is present, Zr concentrations will be most
131 affected, followed by Ti and then Al. As Al is enriched in clay minerals, the Al_2O_3/TiO_2 ratio of
132 fine-grained sediments should increase due to hydrodynamic mineral sorting, if it changes at all.
133 In contrast, as Zr is enriched in sandstones, the Zr/TiO_2 and Zr/Al_2O_3 ratios of fine-grained sedi-
134 ments might decrease due to sedimentary processes. This distinct behavior between the Al_2O_3/TiO_2
135 and Zr/TiO_2 ratios during sediment transport is corroborated by data from suspended and bedload
136 sediments from the Amazon and Ganga rivers (Bouchez *et al.*, 2011; Lupker *et al.*, 2011) (see
137 supplementary Fig. S2), but the question of to what extent such a bias impacts the geochemical
138 record of fine-grained sediments on a 100 Myr timescale is an open question. Using the Al_2O_3,
139 TiO_2 and Zr concentrations together can thus provide clues about the chemical and lithological
140 composition of a sediment's provenance as well as on the effect of mineral sorting on their chemical
141 composition.

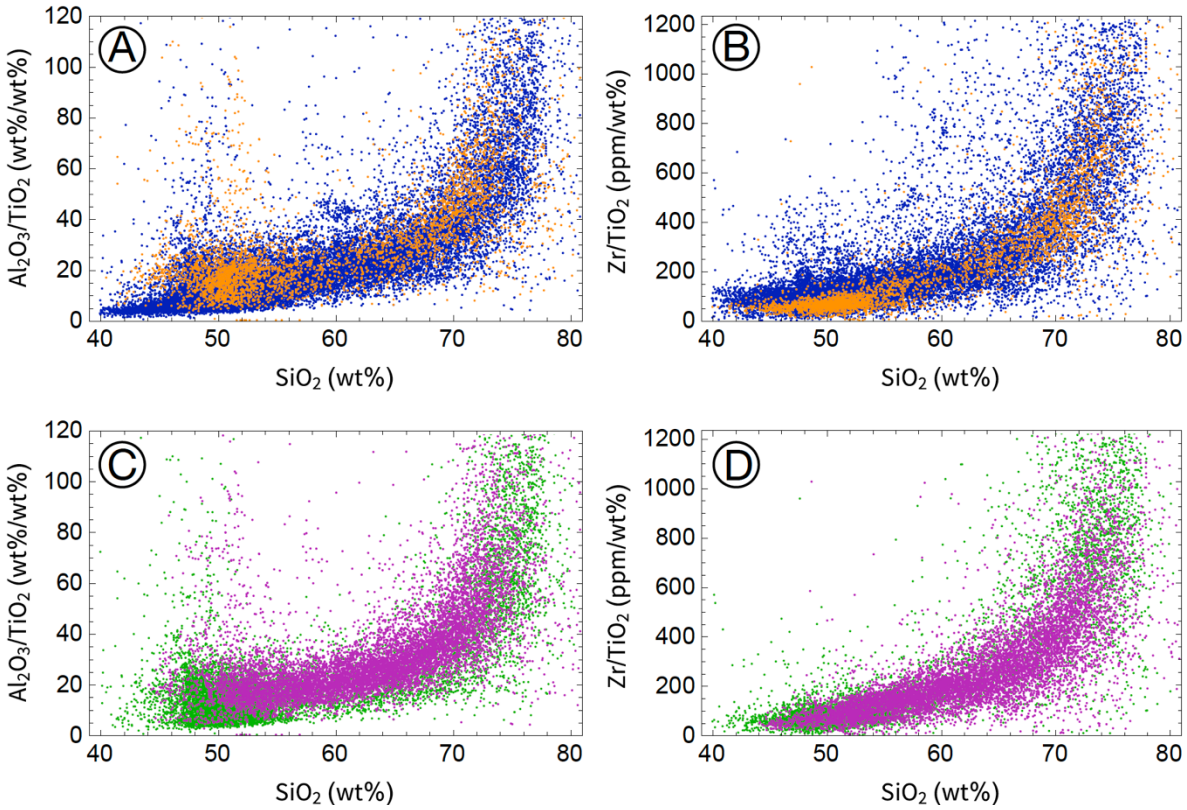

Figure 1. Al_2O_3/TiO_2 and Zr/TiO_2 weight ratios vs. SiO_2 concentrations of rocks from the dataset used in Keller and Schoene (2012), containing a large diversity of plutonic and volcanic lithologies. Only rocks with total oxides between 99 to 101 wt% are considered. A and B: Blue points represent samples younger than 2.5 Gyr and the orange points are samples older than 2.5 Gyr. C and D: Green points represent tholeiitic rocks and purple points are calc-alkaline samples (alkaline rocks are not shown). For more information about the definitions and filtering process for the different magmatic series see supplementary Figure S1. For clarity, the y-axes for the Al_2O_3/TiO_2 and Zr/TiO_2 ratios were cut at 120 and 1200, respectively. Both ratios correlate positively with SiO_2 irrespective of their age and magmatic series. Thus, the Al_2O_3/TiO_2 and Zr/TiO_2 ratios in fine-grained terrigenous sediments convey information on the average rock composition of the sediment provenance.

3 Data compilation, data treatment, and results

Chemical compositions of fine-grained terrigenous sediments were compiled from 63 publications (Supplementary Table S1). This dataset comprises Al_2O_3 (wt%), TiO_2 (wt%) and Zr (µg/g) concentrations of 1437 samples from 191 different localities spanning ages from present to 3.8 Gyr. Q-Q plots show that the Al_2O_3/TiO_2 and Zr/TiO_2 weight ratios depart from normal distributions and are better explained by log-normal distributions (supplementary Figs. S3 and S4). The

159 Al_2O_3/TiO_2 and Zr/TiO_2 ratios were first filtered for outliers using the Chauvenet criterion based
160 on a log-normal distribution. Hereafter, this filtered dataset is named "*individual shale dataset*".
161 After this first outlier rejection step, the Al_2O_3/TiO_2 and Zr/TiO_2 ratios of samples from the same
162 locality and age were averaged to avoid overrepresentation of localities with many samples over
163 those with only few samples. To remove Al_2O_3/TiO_2 and Zr/TiO_2 ratios of sediments with an unu-
164 sual provenance and that do not represent a large-scale sampling of the continents, the averaged
165 ratios were also filtered for outliers using the Chauvenet criterion based on a log-normal distribu-
166 tion. This dataset is named "*averaged shale dataset*".

167 The Al_2O_3/TiO_2 weight ratios (both Al_2O_3 and TiO_2 in wt%) of the "*averaged shale dataset*"
168 range from 38.4 to 12.0 and decrease slightly with time from 26.2 ± 1.3 (2SE; n=56) in the Archean
169 to 22.1 ± 1.1 (2SE; n=47) in the Phanerozoic (Figs. 2 and 3). The Zr/TiO_2 weight ratios (Zr in ppm
170 and TiO_2 in wt%) show more relative dispersion than the Al_2O_3/TiO_2 ratios and range from 73 to
171 585 (Figs. 2 and 3), but exhibit within error constant averages between the Archean (243 ± 24; 2SE,
172 n=55) and Phanerozoic (244 ± 27; 2SE, n=42).

173

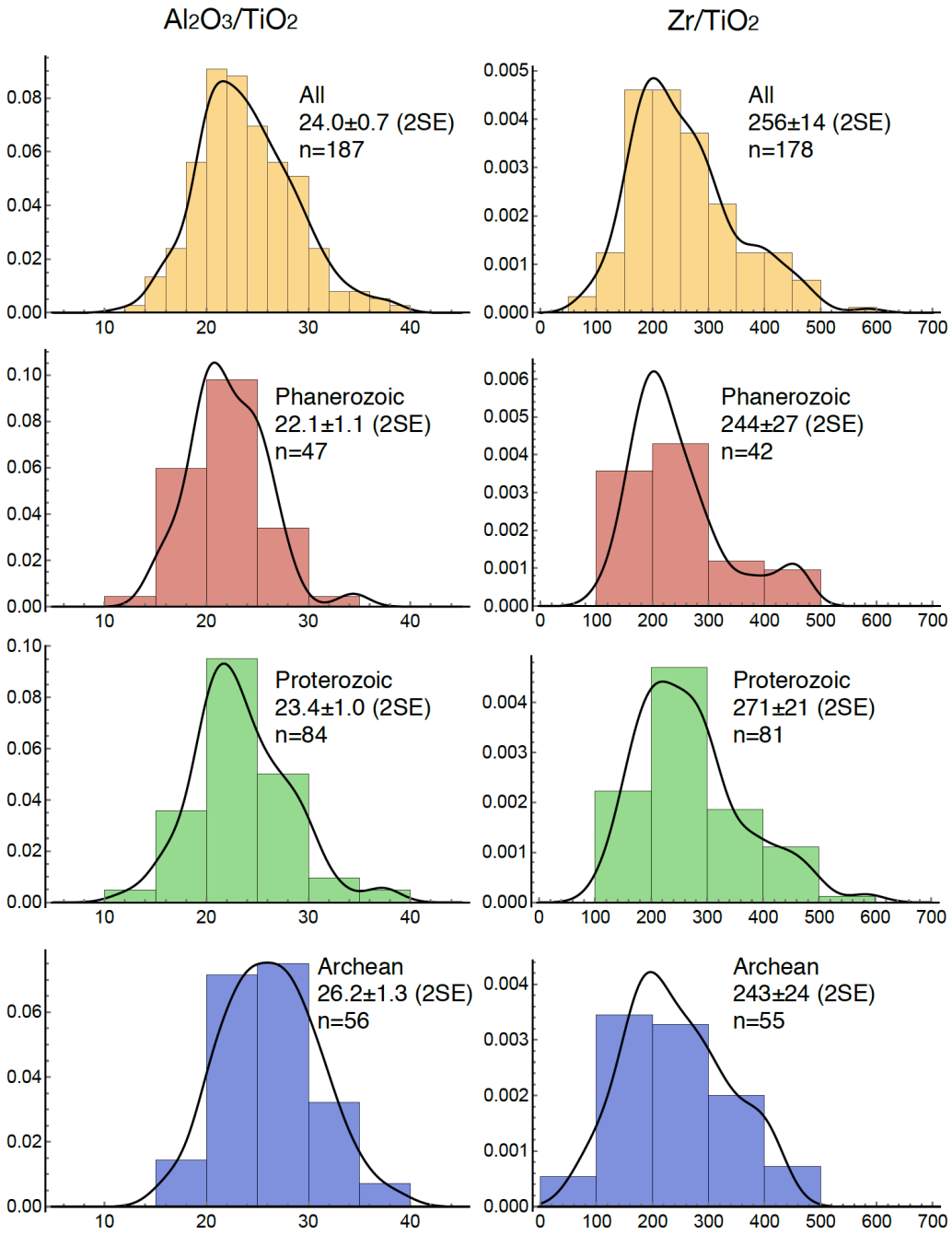

174

175 **Figure 2.** Histograms and Kernel density estimations of filtered and locality averaged Al_2O_3/TiO_2 (left) and
176 Zr/TiO_2 (right) weight ratios of fine-grained terrigenous sediments sorted by age. Indicated in the panels are (*i*)
177 the number of locations that passed all filtering tests (n), (*ii*) the mean, and (*iii*) the 2SE value. While the average
178 Al_2O_3/TiO_2 ratio is slightly decreasing, the average Zr/TiO_2 ratio does not change within error over time.

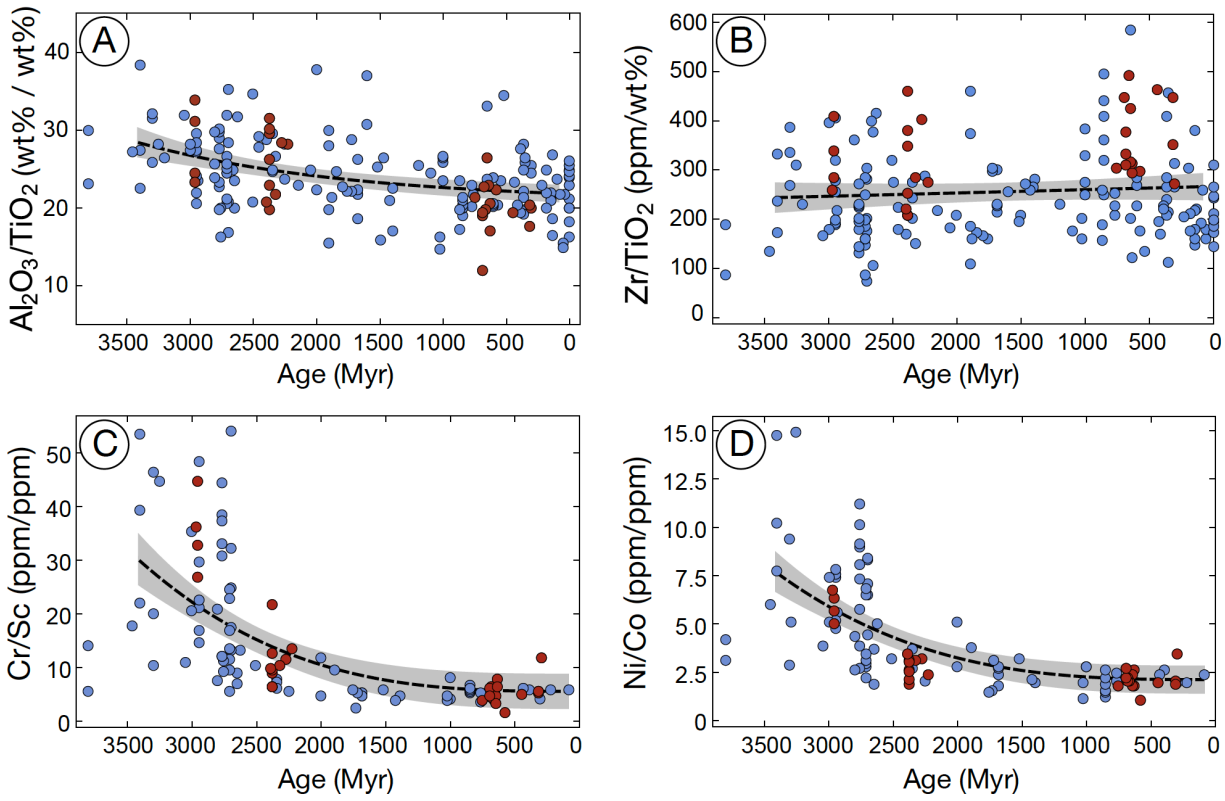

Figure 3. Filtered and locality averaged Al_2O_3/TiO_2 (A), Zr/TiO_2 (B), Cr/Sc (C) and Ni/Co (D) weight ratios of fine-grained terrigenous sediments plotted versus their age. Cr/Sc and Ni/Co ratios are from the compilation of Greber et al., (2017a) and are location-averaged as was done for Al_2O_3/TiO_2 and Zr/TiO_2 ratios. We only consider Ni/Co and Cr/Sc ratios that passed the filter in Greber et al., (2017a), removing samples affected by weathering. Diamictites are highlighted in red while other fine-grained terrigenous sediments are in blue. Indicated are the calculated regressions (black dotted line) the 95% confidence interval of the mean (grey band). The correlation between the Al_2O_3/TiO_2 ratio and age *t* (in Myr) of a sediment can be fitted with a power law $(Al_2O_3/TiO_2)_{Shale}=20.8036+1.00059^t$. The Zr/TiO_2 ratio of fine-grained terrigenous sediments is rather constant and can be fitted with a linear regression $(Zr/TiO_2)_{Shale}=266.614-0.0067 * t$. The Cr/Sc and Ni/Co ratios are fitted with the following formulas: $(Cr/Sc)_{Shale}=5.5253+6.160 * 10^{-10} * t^3$ and $(Ni/Co)_{Shale}=2.1216+1.400 * 10^{-10} * t^3$.

4 Discussion

4.1 Workflow

We first discuss the potential impact of hydrodynamic grain size sorting on the chemical composition of the sediments by evaluating the relative abundances of their Al_2O_3, TiO_2 and Zr concentrations. We then show how the Al_2O_3, TiO_2 and Zr concentrations of fine-grained terrigenous sediments (and their metamorphosed equivalents) are translated into the igneous rock composition of their provenance. To do so, we follow the modelling approach outlined in Greber et al. (2017a), where a set of mass-balance equations are used to solve the measured compositions of the fine-grained terrigenous sediments for the contributions of different igneous rock endmembers. The Al_2O_3/TiO_2 and Zr/TiO_2 ratios are only diagnostic of felsic *vs.* mafic rocks, so to tease apart the contribution of komatiites, we consider ratios involving elements that are relatively compatible in pyroxene and olivine, such as Ni, Co, Cr and Sc (Adam and Green, 2006). All these proxies are insensitive to the presence of chemical sediments like carbonates and banded iron formations on the emerged lands, but as discussed, can be applied to evaluate the relative contribution of different igneous rock types to the sediment record.

To test the applicability of the Al_2O_3/TiO_2 and Zr/TiO_2 ratios of fine-grained terrigenous sediments to reconstruct the composition of their provenance, we first apply our approach to the mid-Phanerozoic crust 250 Myr ago, a time when there are good constrains on the nature of emerged continents. We then calculate the rock composition of the emerged crust 3.25 Gyr ago.

4.2 Evaluating the degree of hydrodynamic mineral sorting over time

Aluminium, Ti and Zr concentrations of sediments have previously been used to evaluate the impact of mineral sorting processes on the chemical composition of sediments (Bouchez *et al.*, 2011; Garcia *et al.*, 1991; 1994; Garzanti *et al.*, 2011; McLennan *et al.*, 1993). Mineral sorting can affect the composition of a sediment by removing dense minerals such as zircon grains into the coarse-grained sediment fraction. On the other hand, recycling of such coarse grained sediments like sandstones can also produce a fine-grained sediment fraction that is enriched in elements normally associated with dense minerals (McLennan *et al.*, 1993). As diamictites are glacial sedimentary deposits, it has been suggested that they are generally less influenced by mineral sorting processes (Gaschnig *et al.*, 2016). While the Al_2O_3/TiO_2, Ni/Co and Cr/Sc ratios of all sediment types in our database largely overlap at any given time during Earth history (Fig. 3), diamictites seem to have in average a higher Zr/TiO_2 ratio compared to non-diamictite sediments (hereafter summarized as shales) and this discrepancy is larger in the Proterozoic and Phanerozoic compared to the Archean (Fig. 3B). This could mean that either both shales and diamictites have been affected by grain size sorting. One of the most sensitive proxies to track hydrodynamic mineral sorting should be the Zr/Al_2O_3 (ppm/wt%) weight ratio, as Al_2O_3 is enriched in fine grained clay minerals and Zr in dense zircon grains. Another advantage of this system is, that mafic and felsic igneous rocks do not exhibit a strong difference in their Zr/Al_2O_3 ratios (supplementary Figure S5). Consequently, if fine-grained terrigenous sediments were significantly impacted by mineral sorting processes, one would expect to observe a difference between the average Zr/Al_2O_3 ratio of the sediments and that of the igneous rock record. We thus calculated the Zr/Al_2O_3 ratio of our already filtered and locality *averaged shale database* by dividing the Zr/TiO_2 with the Al_2O_3/TiO_2 ratio (Table S1). In the Archean, sediments define a rather narrow range in their Zr/Al_2O_3 ratio; diamictites (11.6 ± 2.4; n = 4), shales (9.5 ± 0.9; 2SE, n = 48) and igneous rocks (8.6 ± 0.45; 2SE, n = 2342) overlap within errors (Fig. 4). In the post-Archean, the scatter of the Zr/Al_2O_3 ratio of the sediment and the igneous

240 rock record becomes more pronounced, especially after around 1000 Ma (Figs. 4 and S5). On av-
241 erage, shales younger than 1000 Myr yield a Zr/Al_2O_3 ratio (11.5 ±1.1, 2SE, n=61) that is around
242 9.5 % lower, but still within error identical to that of the contemporary igneous rock record (12.7
243 ± 0.24, n=13096). Diamictites on the other hand define a higher Zr/Al_2O_3 ratio (18.7 ± 3.0, n=15)
244 than igneous rocks. There are various possible explanations for the excess Zr in diamictites, in-
245 cluding that it is an inherited signal from a local source environment that contains igneous rocks
246 with high Zr/Al_2O_3 ratios or that the glacier that produced these diamictites abraded and recycled
247 coarse grained and in zircon-rich sediments (McLennan et al., 1993). To summarize, hydrodynamic
248 mineral sorting had a seemingly small effect on the chemical composition of Archean fine-grained
249 sediments, but it might have become more important over time. The fine-grained sediments that
250 were deposited during the past 1000 Myr show more variation in their Zr/Al_2O_3 ratios. Our dataset
251 is dominated by non-diamictite sediments that seem to be slightly depleted in Zr when compared
252 to the igneous rock record, as is expected from the scavenging of zircon grains into the sand-sized
253 sediment fraction. A consequence is that the linear equation applied to the age versus Zr/TiO_2 cor-
254 relation (Fig. 3B) of the fine-grained sediment record is useful to identify long-term trends in the
255 lithologic composition of the emerged crust, but likely provides a minimum estimate for the pro-
256 portion of felsic rocks in a sediments provenance.

257 To investigate potential changes in the mode of hydrodynamic mineral sorting over Earth's
258 history, we applied a moving median with a step size of 25 Myr and a uniform kernel window
259 width of 250 Myr to the Zr/Al_2O_3 ratio of the non-diamictite sediments. We find that several time
260 intervals of around 200 to 400 Myr width that are characterized by median Zr/Al_2O_3 ratios that are
261 lower than the average composition of the igneous rock record (Fig. 4). Interestingly, the periods
262 defined by low Zr/Al_2O_3 ratios correlate with age peaks in the detrital zircon record of Voice *et al.*,

(2011). It has been shown that these age peaks also broadly correlate with periods of supercontinents (Campbell and Allen, 2008; Hawkesworth *et al.*, 2009; Roberts and Spencer, 2015; Worsley *et al.*, 1984) (Fig. 4). The temporal correlation between peak ages in detrital zircon grains, low Zr/Al_2O_3 ratios in the fine-grained sediment record, and larger landmasses is in agreement with studies that suggest that transport distance and mineral sorting efficiency are positively correlated (Garçon *et al.*, 2013b; Powell, 1998). It is currently debated if the detrital zircon age peaks represent episodic crustal growth due to enhanced magmatic activity (Arndt and Davaille, 2013; Condie *et al.*, 2017), or if they are a preservation bias phenomenon, meaning that rocks related to the collisional mountain building stages of the Wilson-Cycle are better shielded from erosion into the ocean (Cawood and Hawkesworth, 2015; Hawkesworth *et al.*, 2009). We interpret the coincidence of periods with low Zr/Al_2O_3 ratios and zircon age peaks to reflect a sedimentological regime that allowed for an increased production of sandstones and efficient hydrodynamic mineral sorting. In a supercontinent cycle, transport distances from source rocks to marine sediments would be longer and there would be more opportunities for large and dense minerals to be trapped on the continents, as for example in foreland basins and associated lake systems. More work is needed to ascertain the observation that supercontinents are associated with a decrease in the Zr/Al_2O_3 ratio but the present study shows that subtle variations in the geochemistry of terrigenous sediments through time may convey important clues on sediment transport on continents.

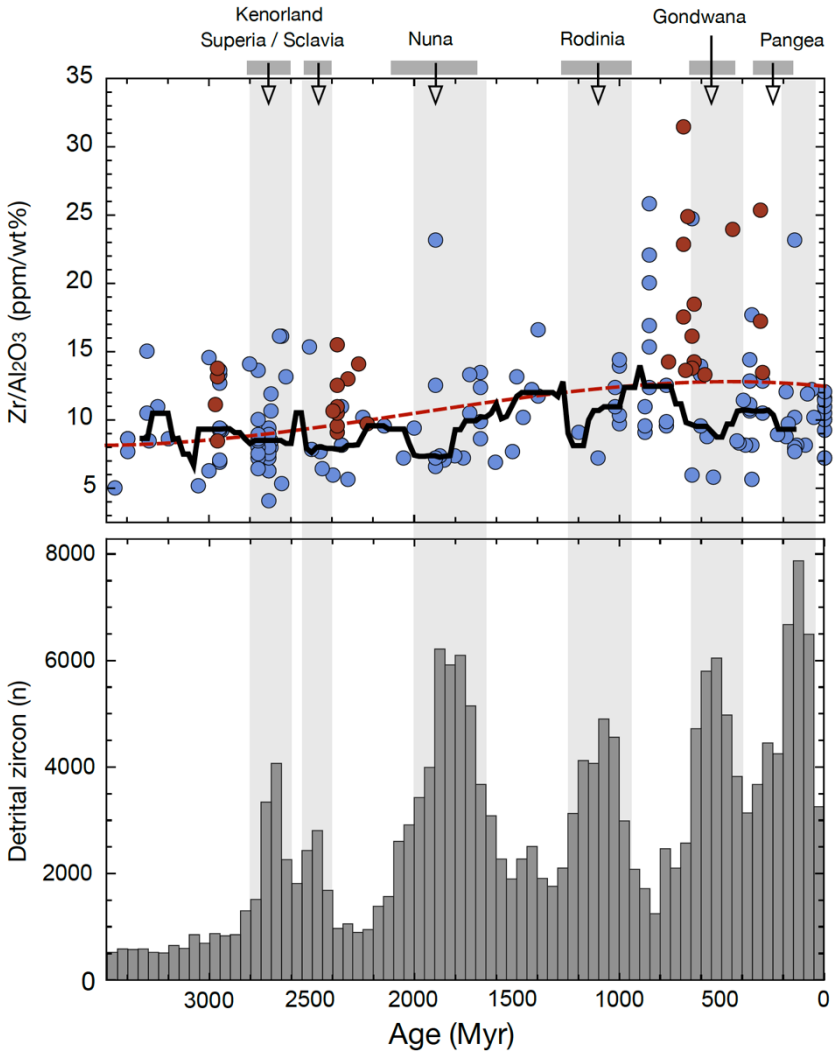

281

282 **Figure 4.** Top: Zr/Al_2O_3 weight ratios of diamictite (red) and non-diamictite samples (blue) from the *averaged*
283 *shale database*. The black line is the moving median with step size of 25 Myr and window width of 250 Myr
284 through the non-diamictite samples (blue circles) to investigate the impact of mineral sorting on the Zr/Al_2O_3
285 ratio of fluvial sediments. The dotted red line is the time dependent average composition of igneous rocks (see
286 Fig. S5). Bottom: detrital zircon age record after Voice et al., (2011). Periods of supercontinent formation are
287 indicated on top of the figure and are based on Cawood and Hawksworth (2015). Periods in which sediments
288 display lower median Zr/Al_2O_3 ratios compared to the mean of igneous rocks seem to be correlated with peaks
289 in the detrital zircon record and supercontinent cycles.

290

4.3 Reconstructing the lithological composition of the mid-Phanerozoic emerged crust

To unravel the nature of the igneous rocks exposed to weathering 250 Myr ago, we first need to define the rock endmembers. Igneous rocks can be broadly divided into ultramafic (<45 wt% SiO_2), mafic (45 - 52 wt% SiO_2; MgO < 18 wt%), intermediate (52 - 63 wt% SiO_2) and felsic rocks (>63 wt% SiO_2) (Le Bas and Streckeisen, 1991). Out of these groups, ultramafic rocks are expected to be of subordinate importance for the Phanerozoic continents. Furthermore, as already indicated by their name, the chemical characteristics of intermediate rocks are in between those of mafic and felsic rocks. Regardless of their formation mechanism, the element composition of intermediate rocks like andesites can effectively be modeled as a mixture of mafic and felsic rocks. Thus, they are not regarded as an individual endmember in our model. Therefore, to reconstruct the lithological composition of the mid-Phanerozoic emerged continents, we limit our endmembers to mafic (subscript M) and felsic rocks (subscript F). The mass fractions of felsic (f_F) and mafic (f_M) components in the 250 Myr old fine-grained terrigenous sediments (and by extension of their provenance) can be calculated using their Al_2O_3/TiO_2 and Zr/TiO_2 ratios and the mass-balance equations:

$$\left(\frac{Al_2O_3}{TiO_2}\right)_{shale} = \frac{f_F[TiO_2]_F\left(\frac{Al_2O_3}{TiO_2}\right)_F + (1-f_F)[TiO_2]_M\left(\frac{Al_2O_3}{TiO_2}\right)_M}{f_F[TiO_2]_F + (1-f_F)[TiO_2]_M}, \quad (1),$$

$$\left(\frac{Zr}{TiO_2}\right)_{shale} = \frac{f_F[TiO_2]_F\left(\frac{Zr}{TiO_2}\right)_F + (1-f_F)[TiO_2]_M\left(\frac{Zr}{TiO_2}\right)_M}{f_F[TiO_2]_F + (1-f_F)[TiO_2]_M}, \quad (2).$$

Greber et al. (2017a) used the Ti isotopic composition of fine-grained terrigenous sediments to calculate the proportions of felsic and mafic rocks in the mid-Phanerozoic emerged crust using a similar mass-balance equation:

$$\delta^{49}Ti_{shale} = \frac{f_F[TiO_2]_F\delta^{49}Ti_F + (1-f_F)[TiO_2]_M\delta^{49}Ti_M}{f_F[TiO_2]_F + (1-f_F)[TiO_2]_M} \quad (3),$$

where $\delta^{49}Ti$ is the Ti isotopic composition expressed as the deviation in permil of the $^{49}Ti/^{47}Ti$ ratio relative to the OL-Ti standard. The weight ratios Th/Sc and La/Sc (both ppm/ppm) are also good indicators of the nature of the sediment provenance (Taylor and McLennan 1985). Thus, we also use the published estimates of the average La/Sc (2.9 ± 0.5; 95% c.i.) and Th/Sc (1.0 ± 0.1; 95% c.i.) ratios of shales of Phanerozoic age (0.6 to 0.0 Gyr) from Taylor and McLennan (1985), to test if our model results are consistent between ratios normalized to Sc and ratios normalized to TiO_2. For those ratios, the mass-balance equations take the form:

$$\left(\frac{La}{Sc}\right)_{shale} = \frac{f_F[Sc]_F\left(\frac{La}{Sc}\right)_F + (1\text{-}f_F)[Sc]_M\left(\frac{La}{Sc}\right)_M}{f_F[Sc]_F + (1\text{-}f_F)[Sc]_M}, \quad (4),$$

$$\left(\frac{Th}{Sc}\right)_{shale} = \frac{f_F[Sc]_F\left(\frac{Th}{Sc}\right)_F + (1\text{-}f_F)[Sc]_M\left(\frac{Th}{Sc}\right)_M}{f_F[Sc]_F + (1\text{-}f_F)[Sc]_M}, \quad (5).$$

As can be seen in equations 1 to 5, next to the composition of the fine-grained terrigenous sediments, the most important input parameters for our model are the concentrations and elemental ratios of the rock endmembers. A potential difficulty in the mass-balance approach in the Phanerozoic is to estimate the composition of the mafic endmember, as mafic rocks from Arc-settings (Arc-basalts) are depleted in some elements such as Ti and Zr compared to within plate basalts (WPB) that include Ocean Island basalts (OIB), continental flood basalts provinces (LIPs) and intra-continental basalts not associated with LIPs (Fig. 4 and Table 1). A compilation of whole rock compositions of WPB and Arc-basalt samples shows that the Al_2O_3/TiO_2 ratios are variable, ranging from low values in OIB and LIP basalts (*e.g.*, Emeishan LIP = 5.1 ± 0.3; 2SE) to high values in Arc-basalts (19.6 ± 0.8; 2SE). The Zr/TiO_2 ratio is more or less constant among these different mafic rocks (Table 1). The depletion of Arc-basalts in Ti and high-field-strength elements in general (HFSE; *e.g.*, Hf, Zr, Ti, Nb, Ta) relative to mid-ocean ridge basalts is well-documented

and has been attributed to the presence of HFSE-rich minerals like rutile or ilmenite in the subduction zone system or to the lower mobility of HFSE in fluids responsible for the metasomatism of the depleted mantle wedge (Kelemen *et al.*, 2014; 1990; Münker *et al.*, 2004; Ulmer, 2001; Woodhead *et al.*, 1998). Furthermore, it was also suggested that the high Ti concentration in OIBs cannot be achieved solely by melting of a peridotitic mantle, but instead requires a small amount of recycled mafic crust in its source (Prytulak and Elliott, 2007). To account for this chemical diversity of modern mafic magmatic rocks, we split the mafic endmember into WPB and Arc-basalts. We note $f_{\mathrm{WPB}} = m_{WPB}/(m_{WPB} + m_{Arc} + m_F)$ and $f_{Arc} = 1 - f_{WPB} - f_F$, the proportions of these endmembers in the sediment provenance. Data from the Emeishan LIP has been used for the Al_2O_3, TiO_2, Zr, La, Th and Sc concentrations of the WPB endmember. The reasoning behind this is that OIB and non-LIP intra-continental basalts are assumed to be volumetrically less important for the Phanerozoic emerged crust compared to LIP and Arc-basalts. Figure 5 shows that mixing between the Emeishan LIP and the calculated average Arc-basalt composition of the PetDB database can explain the composition of all other types of basalt for the ratios that we are interested in (black dotted line in Fig. 5), which is the reason why the composition of the Emeishan LIP is used for the LIP end-member.

One can obtain exact solutions for the proportions of all rock types in the emerged crust (3 unknowns; f_F, f_{Arc}, f_{WPB}) by writing sets of mass-balance equations (*e.g.*, Eqs. 6-7-11, 6-8-11, 6-9-11 or 6-10-11), all involving the Al_2O_3/TiO_2 ratio, which distinguishes between WPB and Arc-basalts (in addition to distinguishing between mafic and felsic rocks), and either the Zr/TiO_2, Th/Sc, La/Sc ratios or δ^{49}Ti value, which distinguish between mafic and felsic rocks:

$$\left(\frac{Al_2O_3}{TiO_2}\right)_{\mathrm{shale}} = \frac{f_F[TiO_2]_F\left(\frac{Al_2O_3}{TiO_2}\right)_F + f_{Arc}[TiO_2]_{Arc}\left(\frac{Al_2O_3}{TiO_2}\right)_{Arc} + f_{WPB}[TiO_2]_{WPB}\left(\frac{Al_2O_3}{TiO_2}\right)_{WPB}}{f_F[TiO2]_F + f_{Arc}[TiO2]_{Arc} + f_{WPB}[TiO2]_{WPB}} \quad (6),$$

$$\left(\frac{Zr}{TiO_2}\right)_{shale} = \frac{f_F[TiO_2]_F\left(\frac{Zr}{TiO_2}\right)_F + f_{Arc}[TiO_2]_{Arc}\left(\frac{Zr}{TiO_2}\right)_{Arc} + f_{WPB}[TiO_2]_{WPB}\left(\frac{Zr}{TiO_2}\right)_{WPB}}{f_F[TiO_2]_F + f_{Arc}[TiO_2]_{Arc} + f_{WPB}[TiO_2]_{WPB}} \quad (7)$$

$$\left(\frac{Th}{Sc}\right)_{shale} = \frac{f_F[Sc]_F\left(\frac{Th}{Sc}\right)_F + f_{Arc}[Sc]_{Arc}\left(\frac{Th}{Sc}\right)_{Arc} + f_{WPB}[Sc]_{WPB}\left(\frac{Th}{Sc}\right)_{WPB}}{f_F[Sc]_F + f_{Arc}[Sc]_{Arc} + f_{WPB}[Sc]_{WPB}} \quad (8)$$

$$\left(\frac{La}{Sc}\right)_{shale} = \frac{f_F[Sc]_F\left(\frac{La}{Sc}\right)_F + f_{Arc}[TiO_2]_{Arc}\left(\frac{La}{Sc}\right)_{Arc} + f_{WPB}[TiO_2]_{WPB}\left(\frac{La}{Sc}\right)_{WPB}}{f_F[Sc]_F + f_{Arc}[Sc]_{Arc} + f_{WPB}[Sc]_{WPB}} \quad (9)$$

$$\delta^{49}Ti_{shale} = \frac{f_F[TiO_2]_F\delta^{49}Ti_F + f_{Arc}[TiO_2]_{Arc}\delta^{49}Ti_{Arc} + f_{WPB}[TiO_2]_{WPB}\delta^{49}Ti_{WPB}}{f_F[TiO_2]_F + f_{Arc}[TiO_2]_{Arc} + f_{WPB}[TiO_2]_{WPB}} \quad (10),$$

$$1 = f_F + f_{Arc} + f_{WPB} \quad (11).$$

All the compositions of the rock endmembers and the fine-grained terrigenous sediments to solve equations 6 to 10 are summarized in supplementary Table S2. The results of the various sets of mass-equations are given in Table 2 and shown in Figure 6. The errors on these estimates are 95% confidence intervals and have been calculated following the methodology outlined in Greber et al. (2017a). The solutions involving the various pairs of proxy ratios all agree within error, indicating that felsic material represented between 67 ± 7 and 84 ± 15 wt% of the emerged crust 250 Myr ago. As expected, the Al_2O_3/TiO_2 - Zr/TiO_2 pair results in the lowest estimate of felsic material because zircon grains can be scavenged into sandstones. The combination of Al_2O_3/TiO_2 and $\delta^{49}Ti$ yields the highest proportion of felsic rocks in the emerged crust 250 Myr ago and the rather large error on this estimate is due to the quasi parallel evolution of these two equations at a high felsic rock fraction (Fig. 6). A small change in the $\delta^{49}Ti$ value of the WPB endmember from +0.005‰ (the average value of basalts from diverse tectonic settings; Millet et al., 2016) to +0.04 ‰ (a plausible value for tholeiitic basalts; Deng et al., 2019), would shift the Ti isotope curve in Figure 6 so that it overlaps with the solutions given by the La/Sc and Th/Sc ratios. Averaging the results of the 5 different systems (Al_2O_3/TiO_2, Zr/TiO_2, La/Sc, Th/Sc and Ti isotopes)

without further corrections indicates that the emerged continents 250 Myr ago consisted of 76 ± 8 wt% felsic rocks, 14 ± 6 wt% Arc-basalts and 10 ± 2 wt% within plate basalts.

This result can be compared to independent estimates of the felsic/mafic rock ratio in the emerged continents based on surface mapping (supplementary Table S3 and gray bar in Figure 6) (Condie, 1993; Dürr *et al.*, 2005; Hartmann and Moosdorf, 2012; Moosdorf *et al.*, 2010; Wedepohl, 1995). Examining mapped mafic and felsic rocks, Condie (1993) and Wedepohl (1995) suggested that the Phanerozoic emerged continents contained 87 and 89 wt% felsic lithologies, respectively. Digital lithological maps of north America (Moosdorf *et al.*, 2010) and Earth as a whole (Dürr *et al.*, 2005; Hartmann and Moosdorf, 2012) suggest a lower proportion of felsic rocks ranging from 61 to 77 wt% (supplementary Table S3). Overall, the felsic/mafic rock ratio in the emerged crust from mapping agrees with our estimate based on the sediment record and shows that our approach does not suffer from any obvious bias and can be applied to test whether the Paleoarchean emerged crust was dominated by mafic lithologies or not.

With regard to Arc-basalts *vs*. WPB contributions to fine-grained marine sediments on the modern Earth, it is to our knowledge the first time that such an estimate is provided. A caveat, however, is that we chose the Emeishan LIP as WPB endmember due to its low Al_2O_3/TiO_2 ratio. Therefore, the contribution of WPB to the sediment flux is likely underestimated. As shown in Fig. 6, our estimate of the felsic and mafic proportions are robust, as the proxy ratio reconstructions show little sensitivity to the abundance of felsic rocks when the ratio WPB/Arc-basalts is higher than ~0.5.

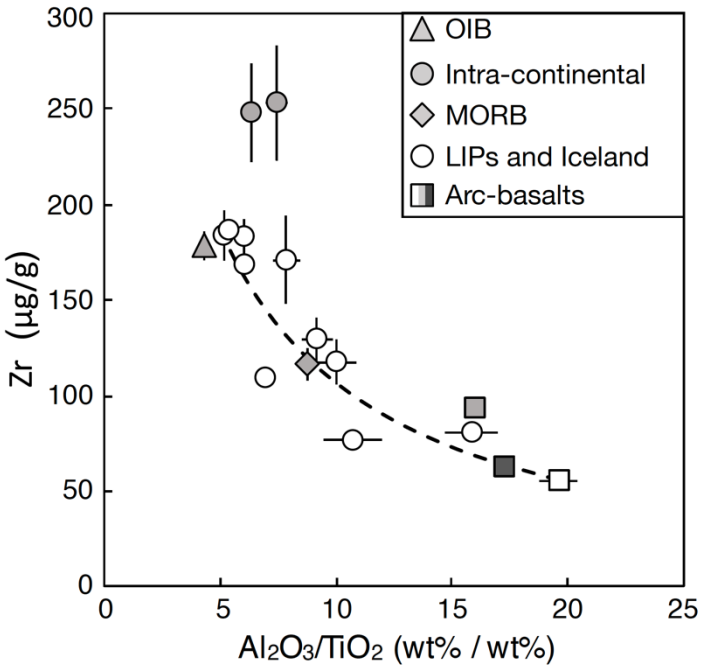

397

398 **Figure 5.** Zirconium concentration *vs.* Al_2O_3/TiO_2 ratio in different types of Phanerozoic mafic rocks. Empty
399 circles are average values for various continental flood basalts (LIPs; *i.e.*, CAMP, Emeishan, Deccan Traps and
400 Parana) calculated from the GeoRoc database and Hooper (2000). The square symbols represent different esti-
401 mates for Arc-basalts; light grey square is the mean of continental Arc-basalts, the dark grey square is the mean
402 of oceanic Arc-basalt (both from Kelemen et al. 2014) and the empty square is the average of Arc-basalt (both
403 continental and oceanic) after the PetDB database. The average composition of MORBs is from Gale et al. (2013),
404 and the two intra-continental basalt examples (Chaîne de Puys, France; Doufutun, central China) are based on
405 Hamelin et al. (2009) and Lie et al. (2015), respectively. The data have been filtered following the criteria outlined
406 in Greber et al. (2017a), *i.e.* only rocks with SiO_2 concentrations between 45 and 52 wt% and MgO < 18wt% and
407 total major element concentrations between 99 and 101 wt% were considered. Errors are 2SE and sometimes
408 smaller than the symbol size. For data and references, see Table 1.
409

410

411

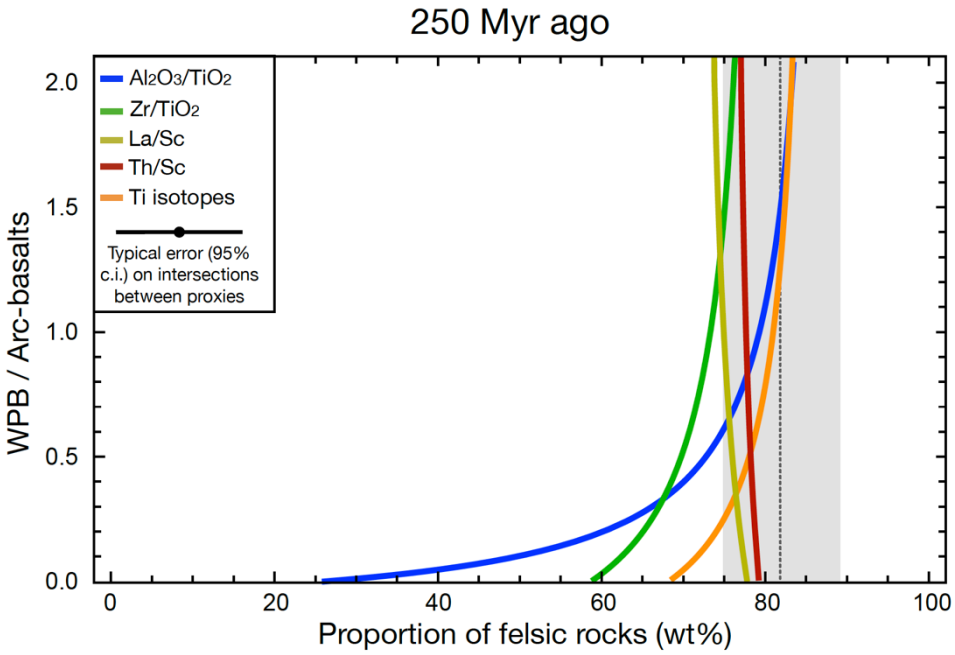

412

413 Figure 6. Calculated proportion of felsic rocks in the emerged crust (x-axis) relative to the ratio of within plate
414 basalts to Arc-basalts (y-axis) that explains the Al_2O_3/TiO_2 (blue), Zr/TiO_2 (green), La/Sc (olive) and Th/Sc (red)
415 and $\delta^{49}Ti$ (orange) values of the Phanerozoic fine-grained terrigenous sediment record (see supplementary Table
416 S2). The grey bar with black dotted line is the mean (82 ± 7 wt%; 2SE, n=4) of different estimates of the abun-
417 dance of felsic rocks in the modern emerged continents based on surface maps (see supplementary Table S3).

418

419 *4.4 Reconstructing the lithological composition of the Paleoarchean emerged crust*

420 The rocks found in the Paleoarchean crust are of different nature than those found more re-
421 cently, calling for a careful assessment of the rock endmembers used in the mixing model. Mafic
422 rocks of Archean age are more homogeneous in their Ti and Zr concentrations than those in the
423 post-Archean (Moyen and Laurent, 2018), so there is no need to divide the mafic endmember into
424 sub-categories. Another distinguishing feature of the Archean crust is the common occurrence of
425 ultramafic komatiitic magmas (Arndt, 2003; Condie and O'Neill, 2011), lavas with a unique chem-
426 ical composition characterized by unusually high Mg, Ni and Cr concentrations. Consequently, to

reconstruct the lithological composition of the emerged crust 3.25 Gyr ago, we rewrite our endmember mixing model to quantify the relative abundances of felsic, mafic and komatiitic (f_K) lithologies. For these calculations, we use (i) the Al_2O_3/TiO_2 (wt%/wt%), Zr/TiO_2 (ppm/wt%), La/Sc (ppm/ppm) and Th/Sc (ppm/ppm) weight ratios, as well as δ^{49}Ti values due to their sensitivities to discriminate between Archean felsic and mafic rocks (Fig. 1 and Greber et al., 2017a) and (ii) the Ni/Co and Cr/Sc ratios as indicators of the contribution of komatiites (Greber et al., 2017a). The following mixing equations can be written:

$$\left(\frac{Al_2O_3}{TiO_2}\right)_{shale} = \frac{f_F[TiO_2]_{F\text{-}A}\left(\frac{Al_2O_3}{TiO_2}\right)_{F\text{-}A} + f_M[TiO_2]_{M\text{-}A}\left(\frac{Al_2O_3}{TiO_2}\right)_{M\text{-}A} + f_K[TiO_2]_K\left(\frac{Al_2O_3}{TiO_2}\right)_K}{f_F[TiO_2]_{F\text{-}A} + f_M[TiO_2]_{M\text{-}A} + f_K[TiO_2]_K} \quad (12),$$

$$\left(\frac{Zr}{TiO_2}\right)_{shale} = \frac{f_F[TiO_2]_{F\text{-}A}\left(\frac{Zr}{TiO_2}\right)_{F\text{-}A} + f_M[TiO_2]_{M\text{-}A}\left(\frac{Zr}{TiO_2}\right)_{M\text{-}A} + f_K[TiO_2]_K\left(\frac{Zr}{TiO_2}\right)_K}{f_F[TiO_2]_{F\text{-}A} + f_M[TiO_2]_{M\text{-}A} + f_K[TiO_2]_K} \quad (13),$$

$$\delta^{49}Ti_{shale} = \frac{f_F[TiO_2]_{F\text{-}A}\delta^{49}Ti_F + f_M[TiO_2]_{M\text{-}A}\delta^{49}Ti_M + f_K[TiO_2]_K\delta^{49}Ti_K}{f_F[TiO_2]_F + f_M[TiO_2]_{M\text{-}A} + f_K[TiO_2]_K} \quad (14),$$

$$\left(\frac{Th}{Sc}\right)_{shale} = \frac{f_F[Sc]_{F\text{-}A}\left(\frac{Th}{Sc}\right)_{F\text{-}A} + f_{M\text{-}A}[Sc]_{M\text{-}A}\left(\frac{Th}{Sc}\right)_{M\text{-}A} + f_K[Sc]_K\left(\frac{Th}{Sc}\right)_K}{f_{F\text{-}A}[Sc]_{F\text{-}A} + f_{M\text{-}A}[Sc]_{M\text{-}A} + f_K[Sc]_K} \quad (15)$$

$$\left(\frac{La}{Sc}\right)_{shale} = \frac{f_F[Sc]_{F\text{-}A}\left(\frac{La}{Sc}\right)_{F\text{-}A} + f_{M\text{-}A}[Sc]_{M\text{-}A}\left(\frac{La}{Sc}\right)_{M\text{-}A} + f_K[Sc]_K\left(\frac{La}{Sc}\right)_K}{f_{F\text{-}A}[Sc]_{F\text{-}A} + f_{M\text{-}A}[Sc]_{M\text{-}A} + f_K[Sc]_K} \quad (16)$$

$$\left(\frac{Ni}{Co}\right)_{shale} = \frac{f_F[Co]_{F\text{-}A}\left(\frac{Ni}{Co}\right)_{F\text{-}A} + f_{M\text{-}A}[Co]_{M\text{-}A}\left(\frac{Ni}{Co}\right)_{M\text{-}A} + f_K[Co]_K\left(\frac{Ni}{Co}\right)_K}{f_{F\text{-}A}[Co]_{F\text{-}A} + f_{M\text{-}A}[Co]_{M\text{-}A} + f_K[Co]_K} \quad (17),$$

$$\left(\frac{Cr}{Sc}\right)_{shale} = \frac{f_F[Sc]_{F\text{-}A}\left(\frac{Cr}{Sc}\right)_{F\text{-}A} + f_{M\text{-}A}[Sc]_{M\text{-}A}\left(\frac{Cr}{Sc}\right)_{M\text{-}A} + f_K[Sc]_K\left(\frac{Cr}{Sc}\right)_K}{f_{F\text{-}A}[Sc]_{F\text{-}A} + f_{M\text{-}A}[Sc]_{M\text{-}A} + f_K[Sc]_K} \quad (18),$$

$$1 = f_F + f_M + f_K \quad (19).$$

Here, subscripts *F-A* and *M-A* indicate the Archean felsic and mafic endmember compositions, which are different from the modern (Keller and Schoene, 2018; 2012). All the parameters needed to solve equations 12 to 19 are presented in supplementary Table S2. The Ni/Co and Cr/Sc ratios of fine-grained sediments of various ages are from the data compilation of Greber et al. (2017a) and we only considered the ratios that passed the filter to remove samples obviously affected by weathering. The samples that did not pass the filter of Greber et al., (2017a) are indicate in *"red"*

449 in the supplementary Table S2. For consistency with the sedimentary Al_2O_3/TiO_2 and Zr/TiO_2 rec-
450 ords, Ni/Co and Cr/Sc ratios of sediments were also averaged by location (see Figure 3C and 3D).

451 We can calculate the proportion of felsic rocks needed in the emerged crust to explain the
452 Al_2O_3/TiO_2, Zr/TiO_2, La/Sc, Th/Sc, δ^{49}Ti, Ni/Co and Cr/Sc signatures of the fine-grained sedi-
453 ments 3.25 Gyr ago, leaving the komatiitic to mafic rock ratio as a free parameter. This is illustrated
454 in Figure 5, where the felsic rock proportion (f_F) of the emerged crust is plotted on the x-axis and
455 the ratio of komatiite to mafic fractions (f_K/f_M) is plotted on the y-axis. The results reveal that the
456 solutions for Al_2O_3/TiO_2, Zr/TiO_2, La/Sc, Th/Sc and δ^{49}Ti plot in a very narrow range and follow
457 steep, subparallel curves. The solution for the Zr/TiO_2 signature of the sediments plots within the
458 range defined by the other proxies and unlike the modern, is not shifted towards a lower proportion
459 of felsic rocks. This agrees with our previous observation that the average Zr/Al_2O_3 ratios of Ar-
460 chean sediments and igneous rocks are within error identical, which suggests that mineral sorting
461 processes during the Archean were limited, at least for the set of terrigenous sediments investigated
462 here. As discussed previously, one factor that controls the degree of zircon sorting into sandstones
463 is the transport regime and transport distance that the sediment grains are subjected to (Garçon *et*
464 *al.*, 2013b). Thus, an explanation for the limited mineral sorting might be that the areal extent of
465 exposed landmasses was small in the Paleoarchean (Bindeman *et al.*, 2018; Flament *et al.*, 2013;
466 Rey and Coltice, 2008). Alternatively, zircon saturation in rocks of Paleoarchean age was likely
467 achieved less frequently 3.25 Gyr ago than in the modern due to higher degrees of partial melting
468 and lower concentrations in incompatible element in mantle-derived magmas (Keller *et al.*, 2017),
469 a matter that would have limited the effect of hydrodynamic grain size sorting on the Zr concen-
470 tration of fine-grained terrigenous sediments.

471 As can be seen in Figure 6, the solution space defined by Cr/Sc and Ni/Co ratios is very differ-
472 ent from that defined by the other proxies. The required amount of felsic rocks to successfully solve

473 equations 17 and 18 and to explain the Cr/Sc and Ni/Co ratios of terrigenous sediments strongly
474 depends on the ratio of komatiitic to mafic rocks in the emerged crust. The solutions of all 7 equa-
475 tions intersect in a small window. The composition of the fine-grained terrigenous sediment record
476 3.25 Gyr ago can only be explained with an emerged crust that contained 65 ± 7 wt% felsic, 25 ±
477 6 wt% mafic and 11 ± 3 wt% komatiitic material (Table 2). This estimate also broadly agrees with
478 the reconstructed composition of the Early Archean emerged crust based on the currently exposed
479 igneous rock record of ~75 wt% felsic rocks and a komatiite to mafic rock ratio of 0.4 (Condie,
480 1993) (yellow star in Figure 6).

481 We tested if a shift in the dominant type of komatiitic rocks (Al-depleted, Al-undepleted, Al-
482 enriched) from the early to the late Archean impacts our model results, by changing the composi-
483 tion of the komatiite endmember. To do so, we used the chemical compositions of the chilled mar-
484 gins from the Komati formation (Al-depleted) and Weltevreden formation (Al-enriched) komatiites
485 from Puchtel et al., (2013). As can be seen in supplementary Figure S6 the nature of the komatiite
486 end-member has no significant influence on the result.

487 Deng et al., (2019) suggested that the Ti isotopic composition of Archean sediments might
488 not be the result of the erosion of a felsic emerged crust, but of continents made with dominantly
489 tholeiitic rocks. We tested this possibility by redefining the element concentrations of our felsic
490 and mafic endmembers using only tholeiitic rocks of Archean age (see Table S2 and Figure S1).
491 As can be seen in Figure S7, applying this new endmember classification, the solutions for the
492 element ratios Al_2O_3/TiO_2, Zr/TiO_2, Th/Sc, and La/Sc show a larger scatter than in our initial model,
493 but still call for a high percentage of igneous felsic material in the Paleoarchean emerged crust
494 (~55wt%). This value agrees within error with the estimate based the Ti isotope proxy of 60 ± 8
495 wt% (see Table 2 and Greber et al., 2017a) and indicates that either tholeiitic magmatic series in
496 the Archean did not produce a significantly different Ti isotope *vs.* SiO_2 trend than calc-alkaline

magmatism, or that the Paleoarchean continents consisted mainly of calc-alkaline rocks. The latter is in agreement with a recent study, suggesting that since 3.8 Gyr calc-alkaline differentiation trends dominated continental magmatism (Keller and Schoene 2018). Therefore, we argue that considering the whole Archean rock catalogue leads to the most reliable definition of the various Archean rock endmembers and translates the sediment record into the lithological composition of the emerged crust most accurately.

At first sight, it might be even counter intuitive that a higher Al_2O_3/TiO_2 ratio of fine-grained terrigenous sediments in the Paleoarchean (~27.7) compared to the Phanerozoic (~22.0) translates into a lower estimate for the proportion of felsic material in the emerged crust. A factor explaining the decreasing trend in the sedimentary Al_2O_3/TiO_2 ratio with time (see Fig. 3A) is the significant increase in the TiO_2 concentration of mafic rocks over Earth's history reflecting lower degrees of melting and associated higher concentrations of highly incompatible elements in more recent mafic magmas (Keller and Schoene, 2018). Because Al_2O_3 is overall more compatible than TiO_2 during mantle melting processes (but not during magmatic differentiation as shown by the increasing Al2O3/TiO2 with increasing SiO2 content; Fig. 1), lower degrees of partial melting shifts the average Al_2O_3/TiO_2 ratio of the continents towards lower values, despite the fact that the amount of mafic rocks did not vary much. The Zr concentration in mafic rocks increases in a similar way as the TiO_2 concentration (Keller and Schoene, 2018), which explains why the Zr/TiO_2 ratio in fine-grained terrigenous sediments does not exhibit the same secular trend as the Al_2O_3/TiO_2 ratio.

The results presented here show that the composition of Paleoarchean fine-grained terrigenous sediments requires an emerged crust with ~65 wt% felsic material (Table 2). The Paleoarchean emerged continents were slightly more mafic and ultramafic compared to their modern counterparts, but to a lesser extent than was suggested previously (Dhuime *et al.*, 2015; Large *et al.*, 2018; Tang *et al.*, 2016). Consequently, the high Ni and Cr concentrations and accompanying high Ni/Co,

Cr/Zn, Cr/U, Cr/Th and Cr/La ratios in 3.25 Gyr old sediments can no longer be taken as evidence for an emerged crust dominated by mafic rocks. Figure 7 indeed reveals that the Ni/Co and Cr/Sc ratios of 3.25 Gyr old fine-grained terrigenous sediments can be explained by an emerged crust that contains 0 to 90 wt% felsic material, depending on the amount of komatiitic rocks present. This means, that the concentrations of Ni and Cr in Paleoarchean sediments are largely controlled by the abundance of ultramafic rocks and komatiites, so these elements are not sensitive proxies to reconstruct the proportion of felsic material in the emerged crust during that time period.

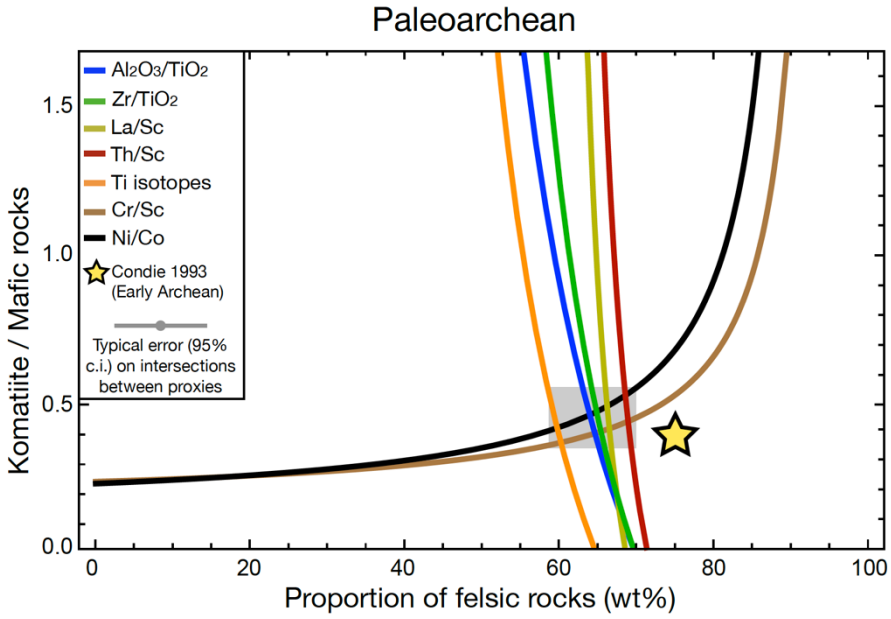

Figure 7. Calculated proportion of felsic rocks in the emerged crust (x-axis) relative to the weight ratio of komatiites to mafic rocks (y-axis) that explains the Al_2O_3/TiO_2 (blue), Zr/TiO_2 (green), La/Sc (olive), Th/Sc (red), $\delta^{49}Ti$ (orange), Ni/Co (black) and Cr/Sc (brown) values of the Paleoarchean fine-grained terrigenous sediment record (Al_2O_3/TiO_2 = 27.7 ± 1.4; Zr/TiO_2 = 245 ± 32; La/Sc = 1.4 ± 0.3; Th/Sc = 0.46 ± 0.09; Ni/Co = 6.9 ± 0.9; Cr/Sc = 26.7 ± 4.0 and $\delta^{49}Ti$ = 0.160±0.023‰, see supplementary Table S2). All seven proxies intersect in a common narrow window (grey box), indicating that the emerged crust 3.25 Gyr ago contained approximately 65 wt% felsic material. The yellow star is the estimate from Condi (1993) based on mapping Early Archean terranes.

4.5 Regional diversity in the lithological makeup of Archean continents

The new dataset of terrigenous sediment compositions allows us to investigate whether regional variations existed in the lithological composition of the Archean continents. To do so, we subdivided the Archean sediments of our averaged shale database into samples from (*1*) Southern Africa (Zimbabwe, South Africa), (*2*) North America - Greenland, (*3*) Australia, (*4*) India and (*5*) Ukraine, and plotted them in the Cr/Sc – Al_2O_3/TiO_2 diagram (Figure 8). The sediment data are encompassed by the ternary mixing space defined by the felsic, mafic and komatiite end-members. There is no obvious trend towards a more felsic composition of the emerged continents from the Paleoarchean (squares) to the Meso- and Neoarchean (circles). As seen from this diagram, the broad secular trend in the chemical composition of terrigenous sediments used to reconstruct the nature of the continents through time (this study; Tang et al., 2016; Greber et al., 2017a; Smit and Mezger 2017) hides a lot of regional diversity. While the data points define an average Archean crust comprising around 60 % felsic, 30 % mafic, and 10 % komatiite rocks, the contributions of these end-members to individual shale localities shows a lot of variation with komatiite contributions that vary between ~0 and 50 % and felsic fractions between 0 and 90%. There does not seem to be any systematics from craton to craton in the proportions of felsic to mafic rocks. The variations seem to be primarily driven by the random distribution of mafic and felsic rocks in a given drainage basin. There is however some systematic craton-to-craton variation in the fraction of komatiites. Sediments sampled in the South Africa craton incorporated of a larger fraction of komatiites than average, while the Indian craton is characterized by a lower komatiite fraction than average. This finding is corroborated by the observation of Taylor and McLennan (1985) that the Archean greenstone belts

560 from Barberton (South Africa) and from the Yilgarn Block (Australia) contain the highest abun-
561 dance of komatiitic material.

562

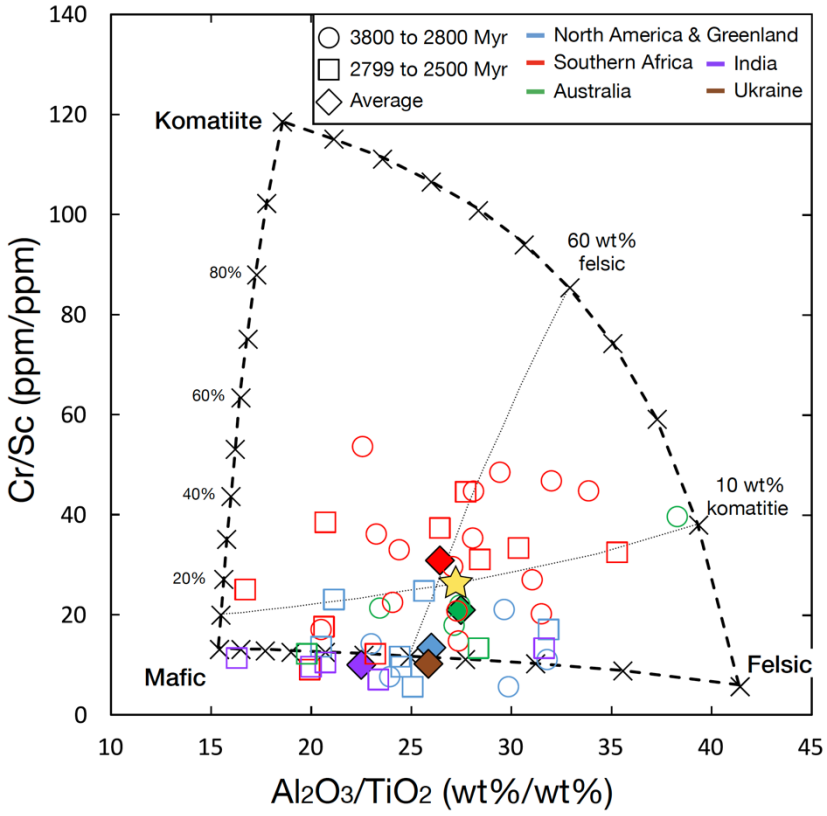

563

564 **Figure 8.** Cr/Sc *vs*. Al_2O_3/TiO_2 ratios of location-averaged samples of Archean age (3.8 to 2.5 Gyr), color coded
565 according to their origin and shape coded according to their age. Indicated in coarse dotted lines is the mixing
566 space defined by the felsic, mafic and komatiitic endmembers, with crosses marking each 10% mixing step.
567 Small dotted lines correspond to a provenance with 60 wt% felsic and 10 wt% komatiitic components. Filled
568 diamonds are the mean values of each location. The yellow star is the result of our endmember model for the
569 emerged crust 3.25 Gyr ago.

570

571

572

4.6 Insights into Paleoarchean geodynamics

The question of the prevailing mode of tectonism during different periods of Earth's history has long been debated (see the following papers for an overview of the present state of this debate: Cawood *et al.*, 2018; Foley, 2018; Hawkesworth and Brown, 2018; Korenaga, 2018; Lenardic, 2018). It is generally accepted that magmatism and other associated processes in subduction zone systems produce felsic lithologies (Barbarin, 1999; Grove *et al.*, 2012; Jagoutz, 2010; Jagoutz *et al.*, 2009; Moyen and Martin, 2012). In modern settings, the transport of water into the mantle via subduction zones can lead to:

(i) Metasomatism and melting of the mantle wedge through dehydration of the slab, producing basaltic melts. These melts are then modified through fractional crystallization, mixing, and assimilation during their ascent towards the surface, resulting in the production of felsic lithologies (Annen *et al.*, 2005; Hildreth and Moorbath, 1988; Müntener and Ulmer, 2018). This leads to the segregation between shallow felsic and deep mafic lithologies. To finally produce a bulk continental crust of andesitic composition, additional processes such as delamination of lower crust mafic litholgies need to be at work (Jagoutz and Kelemen, 2015; Rudnick and Gao, 2003).

(ii) In hot subduction settings, the hot and hydrated subducting slab itself can melt, producing rare felsic rocks named adakites (Defant and Drummond, 1990). A similar mechanism involving partial melting of hydrated subducted slabs in the presence of amphibole and/or garnet may have produced felsic Archean TTGs (Foley *et al.*, 2002; Moyen and Martin, 2012).

In either case (*i* or *ii*), significant volumes of felsic rocks are expected to be produced in a subduction zone setting. Thus, a prominent line of argument for the absence of plate tectonics on Earth

596 until 3.0 Gyr is based on the claim that the continental crust until that time was dominated by mafic
597 rocks (Dhuime *et al.*, 2015; Tang *et al.*, 2016).

598 The composition of the terrigenous sediments has not been the only line of evidence used
599 to argue for predominantly mafic continents in the Paleoarchean. Dhuime et al., (2015) used the
600 Sm-Nd and Sr isotopic compositions of igneous rocks to estimate the average Rb/Sr ratio of the
601 "juvenile continental crust" (the composition of mantle-derived magma that crystallized in the crust
602 after differentiation). For a given igneous rock of a given age and initial $^{143}Nd/^{144}Nd$ and $^{87}Sr/^{86}Sr$
603 ratios, they calculate a model age of crustal extraction from a depleted mantle source using ^{147}Sm-
604 ^{143}Nd systematics. They then calculate the Rb/Sr ratio needed to bring the $^{87}Sr/^{86}Sr$ ratio from a
605 depleted mantle value at the time of extraction (model age given by ^{147}Sm-^{143}Nd) to the initial value
606 measured at the time of crystallization. As the Rb/Sr of igneous rocks correlates positively with
607 their SiO_2 concentration, the observed increase in the Rb/Sr ratio of juvenile continental crust from
608 3 to 2 Gyr was taken as evidence that the composition of the continental crust changed from mafic
609 to andesitic over that time period (Dhuime *et al.*, 2015). The findings of a bulk mafic continental
610 crust (SiO_2 ~49 wt%) prior to 3.0 Gyr is at odds with the currently exposed rock record of that time
611 (Condie, 1993). A solution to this problem could be, that large parts of the mafic lithologies were
612 eroded and are no longer present. However, as shown by Greber et al., (2017a) and the present
613 study, such a process is not recorded in terrigenous sediments. There are two potential issues with
614 the reconstruction of Dhuime et al. (2015) based on ^{87}Rb-^{86}Sr and ^{147}Sm-^{143}Nd systematics of ig-
615 neous rocks:

616 (i) As seen in Figure 9A, most of the interpretation about the composition of the continents for
617 the time prior to 3.0 Gyr (*i.e.*, samples with mantel extraction model ages $T_{DM} \geq 3.0$ Gyr) relies
618 on rocks that crystallized within the last 500 Myr (*i.e.*, crystallization age $t_{CA} \leq 500$ Myr). Al-

most all of them have low modelled Rb/Sr ratios. Thus, for the model to work, one has to assume that the Sm-Nd and Rb-Sr systematics evolved as closed systems and remained undisturbed over billions of years despite magmatic and/or metamorphic reworking.

(ii) The calculated Sm-Nd mantle extraction model ages assume that all rocks were derived from a depleted mantle reservoir. The depleted mantle, however, is an extreme endmember that can bias the mantle extraction ages towards higher values. For example, in the study of Dhuime et al. (2015) rocks from the Deccan Traps flood basalts (~65 Myr) (Vanderkluysen *et al.*, 2011) and basalts from the Kerguelen Archipelago (~25 Myr) (Doucet et al., 2005) were used. In both cases, the ages of these rocks should be similar to their mantle extraction ages. However, applying the mantle extraction age calculation of Dhuime et al. (2015) results in T_{DM} ranging from 819 to 1190 Myr for samples from the Kerguelen system and from 1010 to 4366 Myr for samples from the Deccan Trap basalts. In both cases, their mantle extraction ages are overestimated, which leads to a gross underestimation of the Rb/Sr ratio of the juvenile continental crust. Indeed, an older mantle extraction age will mean more time to produce radiogenic ^{87}Sr so a lower Rb/Sr ratio in the juvenile continental crust is called for to explain a given initial $^{87}Sr/^{86}Sr$ ratio at crystallization. This issue is illustrated in Fig. 9B, where the modelled Rb/Sr ratio is plotted as a function of the crystallization age of the rocks with a T_{DM} of ≥ 3.0 Gyr, *i.e.* data that is used to constrain the Rb/Sr ratio of juvenile continental crust added to the continents before 3.0 Gyr (supplementary material 1 of Dhuime et al. 2015). As can be seen, rocks that crystallized within the last 500 Myr yield lower modelled median Rb/Sr ratios than rocks of older age. The median Rb/Sr model ratio of rocks that crystallized in the Archean (t_{CA} ≥ 2.5 Ga) and are thus likely the samples least affected by the problems outlined above is 0.088. This ratio translates into SiO_2 concentration of ~57 wt%, close to the average SiO_2 concentration of the modern bulk continental crust of Rudnick and Gao (2003) of 60.6 wt%.

643 Based on the combined use of Ni/Co and δ^{49}Ti measurements of fine-grained terrigenous
644 sediments, we previously concluded that the crust was predominantly felsic in the Archean. The
645 present study shows that available concentration data for Al, Ti, Zr, Th, La, Ni, Co, Cr and Sc in
646 fine-grained terrigenous sediments corroborate this conclusion. It also agrees with the inventory of
647 exposed Early Archean igneous rocks (Condie, 1993). Following the argument of Tang et al., (2016)
648 and Dhuime et al., (2015), our findings of a predominantly felsic crust since 3.25 Ga would support
649 the view that subduction-zones were already active at that time.

650 The argument has been made, however, that chemically evolved continents could be formed
651 without subduction zones. The Archean rocks of the Pilbara Craton in Australia are often put for-
652 ward as an example of how felsic rocks in the Archean were produced in thick volcanic plateau
653 complexes (Van Kranendonk *et al.*, 2015). However, it is unclear if these settings are capable of
654 producing an emerged continental crust that contained in average 65 wt% of felsic material. A
655 petrological–thermomechanical numerical model investigating the formation of continental crust
656 via drip tectonics estimated a ratio of felsic to mafic rocks in granite-greenstone terranes of 1.2
657 (Sizova *et al.*, 2015). This is a factor of 2 lower than the ratio of 2.6 estimated in this study that
658 represents the composition of the emerged continents, and a factor of 3.5 lower than the ratio ob-
659 served in currently exposed Early Archean terranes (Condie 1993). The latter value might be more
660 representative of deeper parts of Early Archean continents due to the effect of erosion.

661 To summarize, the lithological and chemical composition of the Paleoarchean emerged
662 crust should no longer be used as argument against the existence of subduction zones at that time.
663 Indeed, the geochemistry of terrigenous sediments of Paleoarchean age points to exposed rocks at
664 the surface of continents that were predominantly felsic; supporting the view that some form of
665 subduction processes were operating since the early Archean (Hopkins *et al.*, 2010; Polat *et al.*,
666 2015; Reimink *et al.*, 2018; Smart *et al.*, 2016).

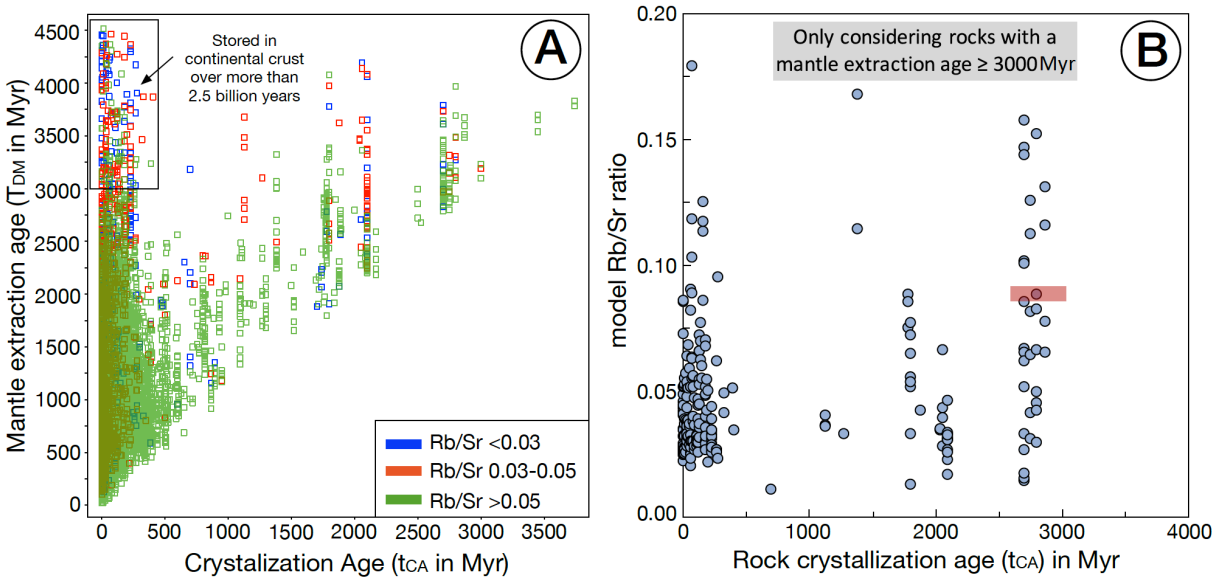

Figure 9. Reevaluation of the data used in Dhuime et al. (2015) (supplementary information Excel file 1). (A) Mantle extraction age based on Sm-Nd isotope systematic *vs*. crystallization age of the rocks, color coded after calculated juvenile Rb/Sr ratios. A large fraction of the low Rb/Sr weight ratios for the pre-3.0 Gyr juvenile continental crust derives from rocks that apparently resided in the continental crust for more than 2.5 Ga. We argue that the very old mantle extraction ages (>3.0 Gyr) of young rocks (<500 Myr) are overestimates resulting from the assumption that their mantle source was depleted. (B) Modelled Rb/Sr ratio of juvenile continental crust *vs*. crystallization age of the rocks with a mantle extraction age of ≥ 3.0 Gyr. It can be seen that rocks with a young crystallization age have lower modelled Rb/Sr ratios. The red bar is the median Rb/Sr ratio (0.088) of rocks with a crystallization age of above 2.5 Gyr.

5 Conclusions

A new compilation of Al_2O_3, TiO_2 and Zr concentrations of fine-grained terrigenous sediments was used to quantify the rock composition of the emerged crust 3.25 Gyr ago. We show that the composition of detrital sediments in the Paleoarchean is best explained with the presence of ~65 wt% felsic rocks and ~11 wt% komatiitic and/or ultramafic material in the emerged crust.

From our estimate, the proportion of mafic and ultramafic rocks decreased from around 35 to 24 wt% from the Archean to the Proterozoic. This shift is smaller than what was advocated previously and we argue that the emerged continents 3.25 Gyr ago were already chemically mature, a result that supports the operation of some form of subduction at that time.

We also used the Zr/Al_2O_3 ratio of the sediments to investigate whether or not hydrodynamic mineral sorting influenced their composition. We find that Archean samples were only marginally impacted by such processes. However, there might be a temporal correlation between time intervals with low Zr/Al_2O_3 ratios in fine-grained sediments and periods of supercontinents, indicating the possibility that large landmasses and mountain building processes led to enhanced continental storage of dense minerals like zircons during those times.

Acknowledgments

The authors thank Matouš Ptáček, Andrey Bekker, Ilya Bindeman and Josh Davies for discussions. Reviews by two anonymous referees and Christopher Spencer substantially improved the quality of the manuscript. NDG was funded by the Swiss National Science Foundation (project number 162341). ND was supported by NASA grants NNX17AE86G (LARS), NNX17AE87G (Emerging Worlds), and 80NSSC17K0744 (Habitable Worlds).

Supplementary Figures

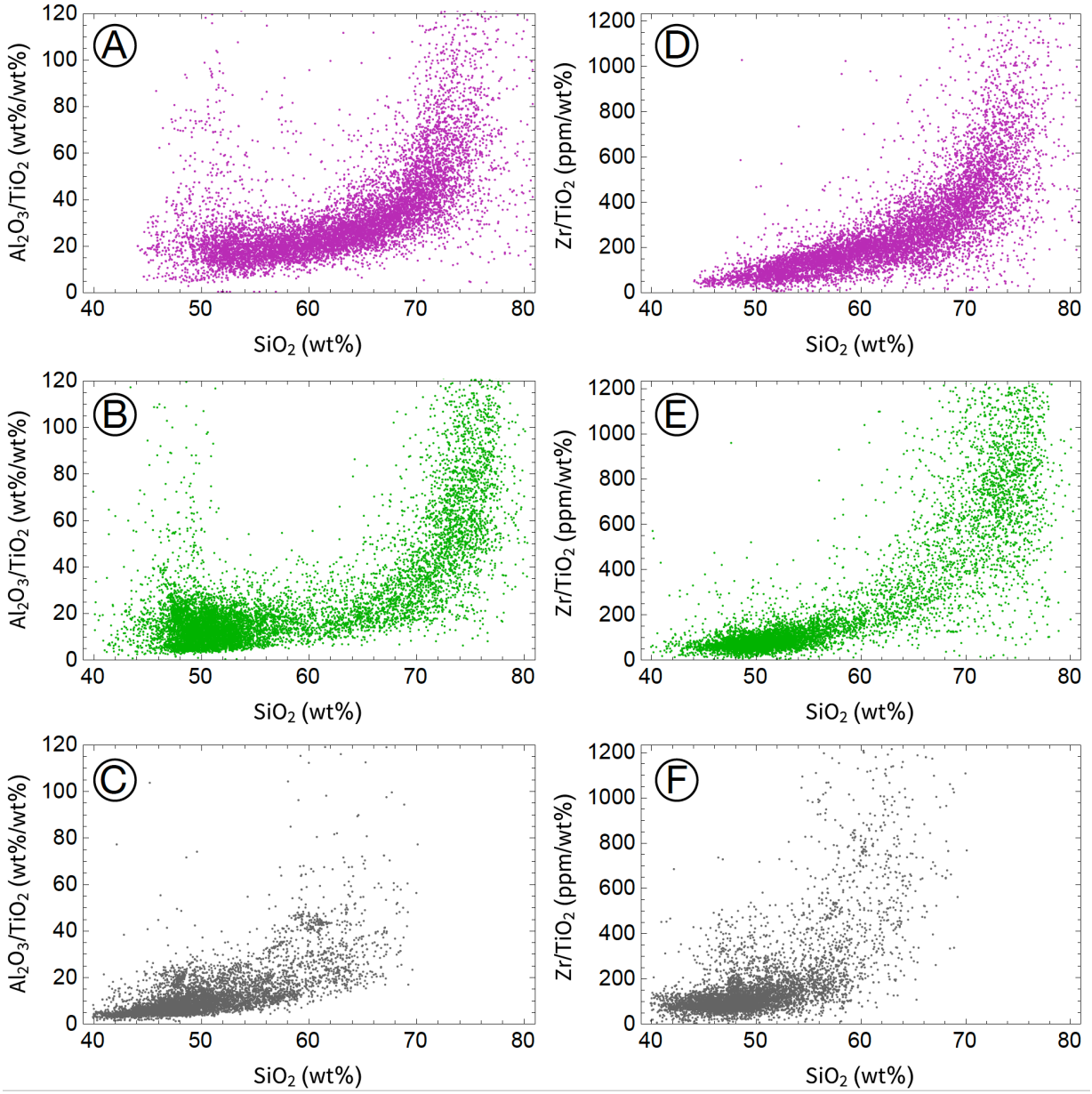

Figure S1. Panels A, B and C display Al_2O_3/TiO_2 ratios *vs*. SiO_2 concentrations of calc-alkaline (A), tholeiitic (B) and alkaline (C) rocks. Panels D, E and F display Zr/TiO_2 ratios *vs*. SiO_2 concentrations of calc-alkaline (D), tholeiitic (E) and alkaline (F) rocks. Data is from the compilation of Keller and Schoene (2012). Only rocks with total oxides between 99 to 101 wt% are considered. Igneous rocks were sorted into alkaline and subalkaline series based on their $Na_2O + K_2O$ and SiO_2 concentrations (wt%) after MacDonald and Katsura (1964). The subalkaline rocks were subdivided into tholeiitic and calc-alkaline series by considering their FeO_T/MgO weight ratios and

710 SiO_2 concentrations (wt%) following Miyashiro (1974). Using the definition for alkaline, tholeiitic and calc-
711 alkaline rocks of Irvine and Baragar (1971) (division of subalkaline rocks is based on an alkali-iron-magnesium
712 -AFM- diagram), most of the SiO_2 rich tholeiitic rocks would enter the calc-alkaline field. However, irrespective
713 of the definitions chosen, the three magmatic series always exhibit positive correlations between the Al_2O_3/TiO_2
714 and Zr/TiO_2 ratios *vs*. SiO_2 concentrations.

715

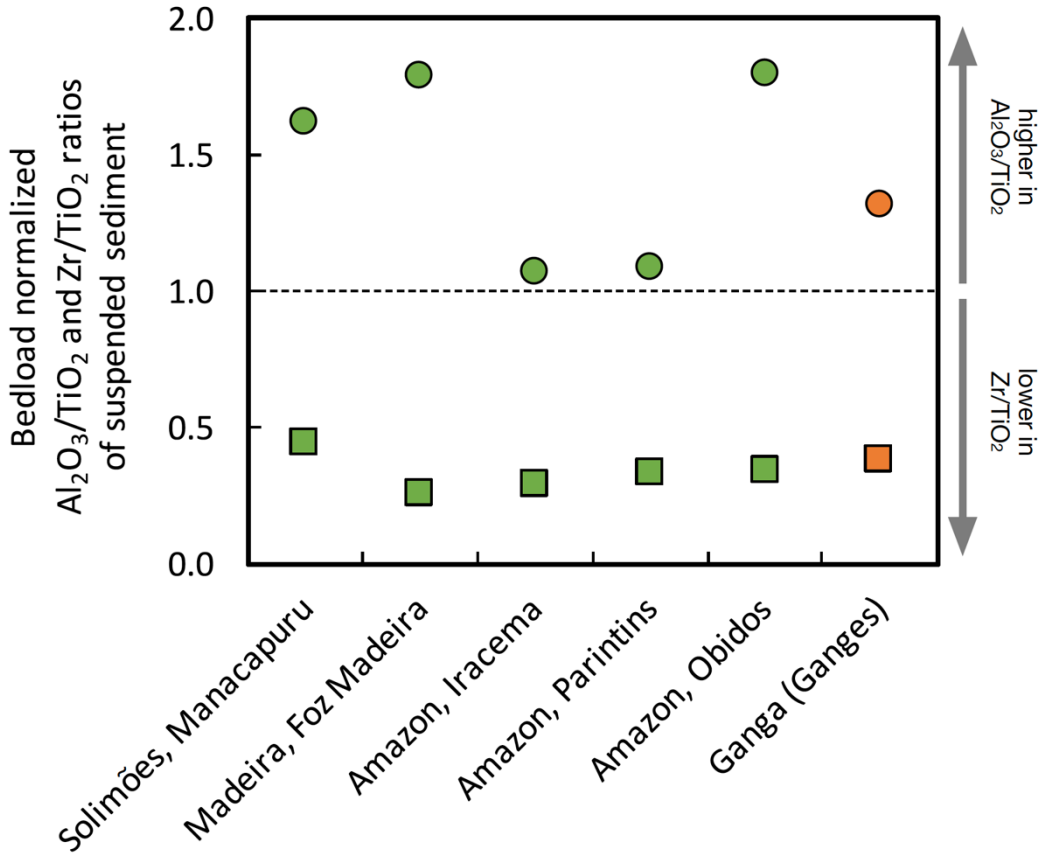

Figure S2. Al_2O_3/TiO_2 weight ratios (circles) and Zr/TiO_2 weight ratios (squares) of the suspended sediment fraction normalized to the composition of the bedload from tributaries to the Amazon (Solimões and Madeira) as well as the Amazon and the Ganges rivers. Al_2O_3/TiO_2 ratios in the suspended load are either higher or close to that of the bedload. Zr/TiO_2 ratios in the suspended load are always lower when compared to the bedload. Relative to Ti (presumably in oxides), Zr is preferentially kept in the bedload (presumably in zircon), while Al is preferentially transported in the suspended sediment fraction (presumably in clays). Data is from Bouchez et al. (2011) and Lupker et al. (2011).

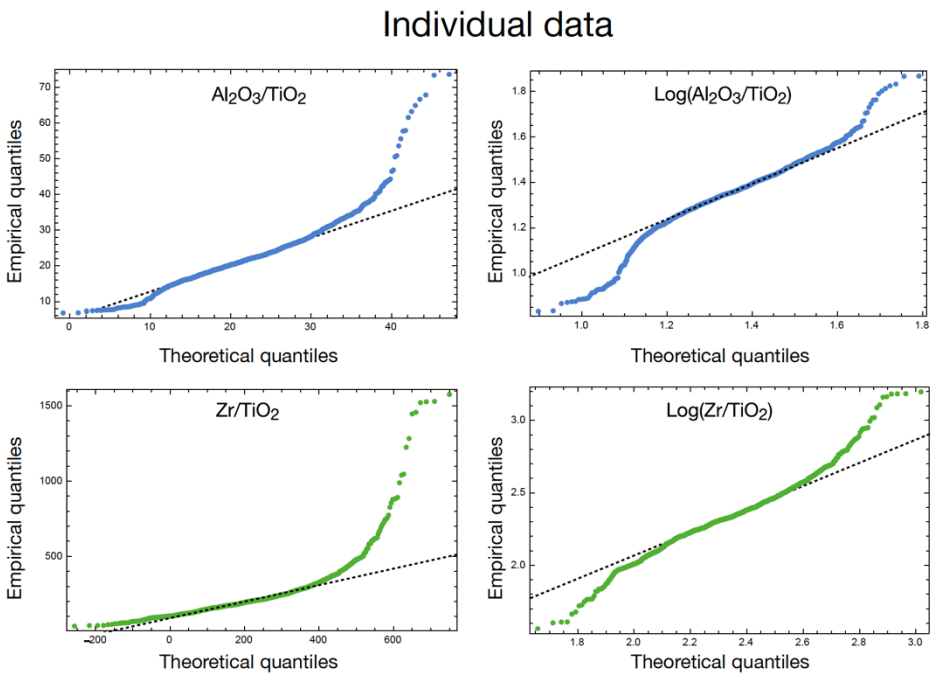

Figure S3. Q-Q-Plots of the "individual shale database".

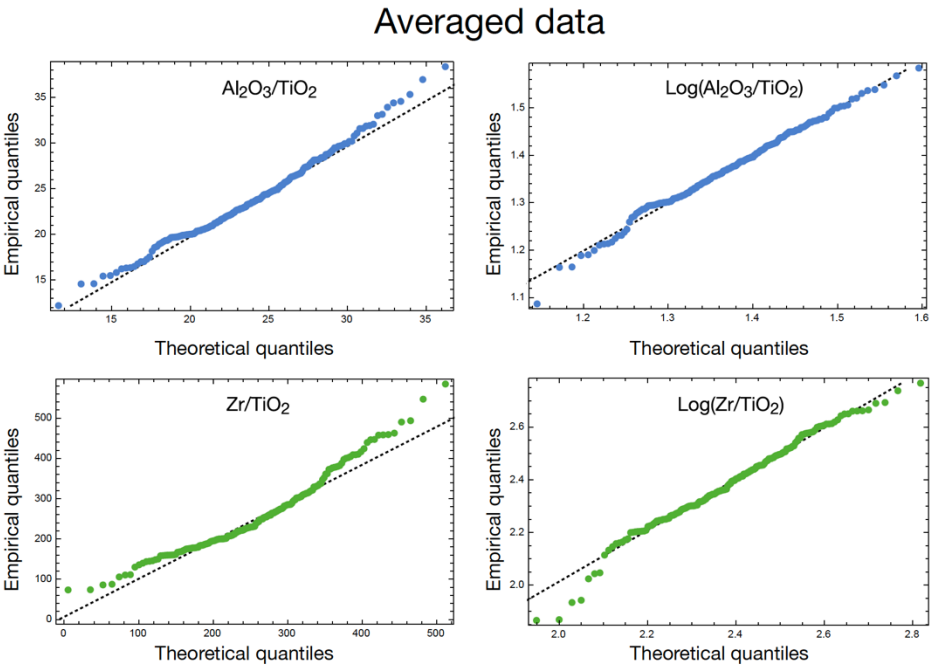

Figure S4. Q-Q-Plots of the "averaged shale database". The slight departure of a few samples from the log-normal law might be due to higher measurement errors at low Zr concentrations or a stronger impact of grain size sorting on these sediments.

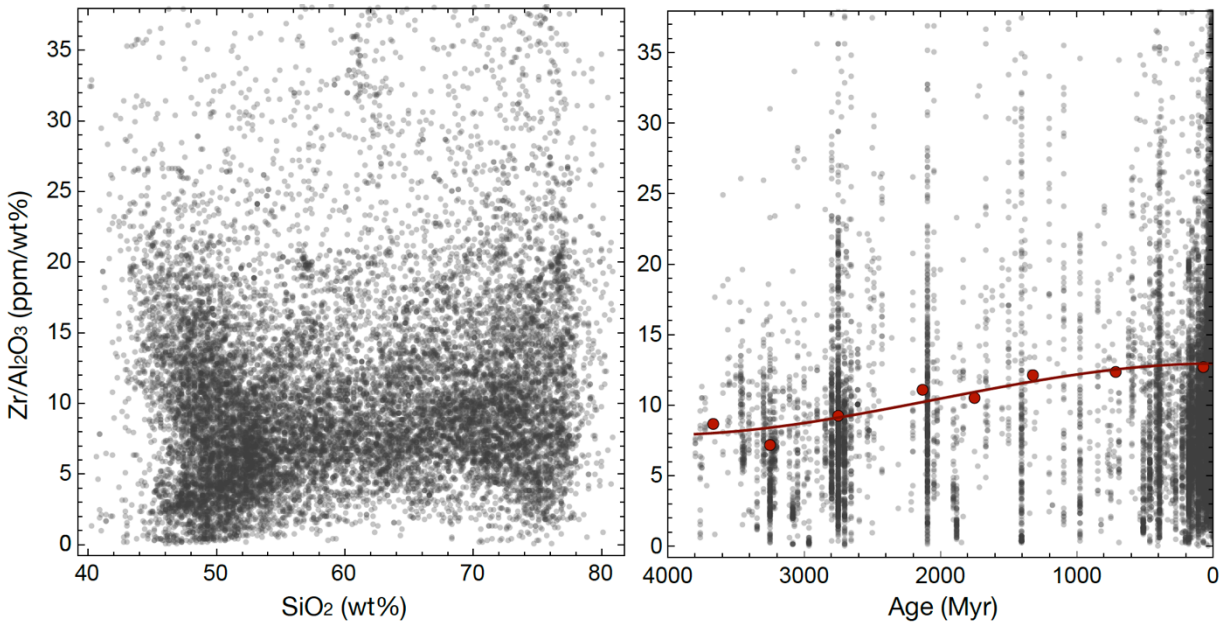

Figure S5. Left: Zr/Al_2O_3 weight ratios of igneous rocks plotted *vs.* SiO_2 concentration. A slight positive correlation between these two parameters can be observed. For clarity, y-axis has been cut at a Zr/Al_2O_3 value of 38. Right: Zr/Al_2O_3 *vs*. age of all igneous rocks. Red line is a correlation through average values calculated at 500 Myr intervals (red circles), which can be fitted using a polynomial $Zr/Al_2O_3 = 12.478 + 0.001538t - 1.8927 * 10^{-6}t^2 + 3.1439 * 10^{-10}t^3$, with *t* the age in Myr. Data is from Keller and Schoene (2012).

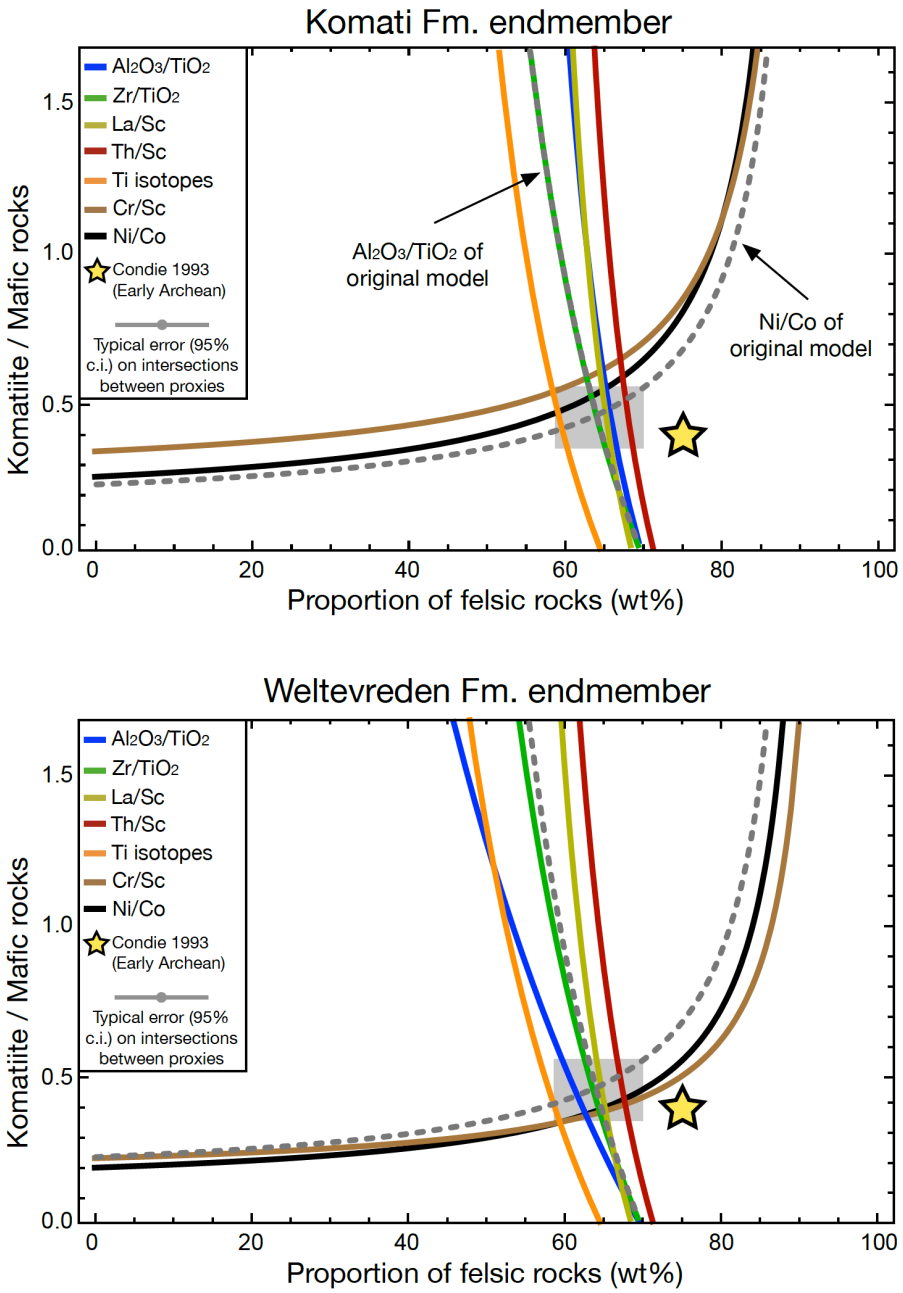

742

743 **Figure S6.** Tests to evaluate if changing the composition of the komatiite end-member influences the recon-
744 structed crust composition. The end-member komatiite compositions considered are the Al-depleted Komati For-
745 mation (top panel) and Al-enriched Weltevreden Formation (bottom panel). The grey dotted lines are the rela-
746 tionships established based on Ni/Co and Al_2O_3/TiO_2 ratios using the average composition of all komatiites.
747 Changing the composition of the komatiite endmember does not significantly influence the results.

748

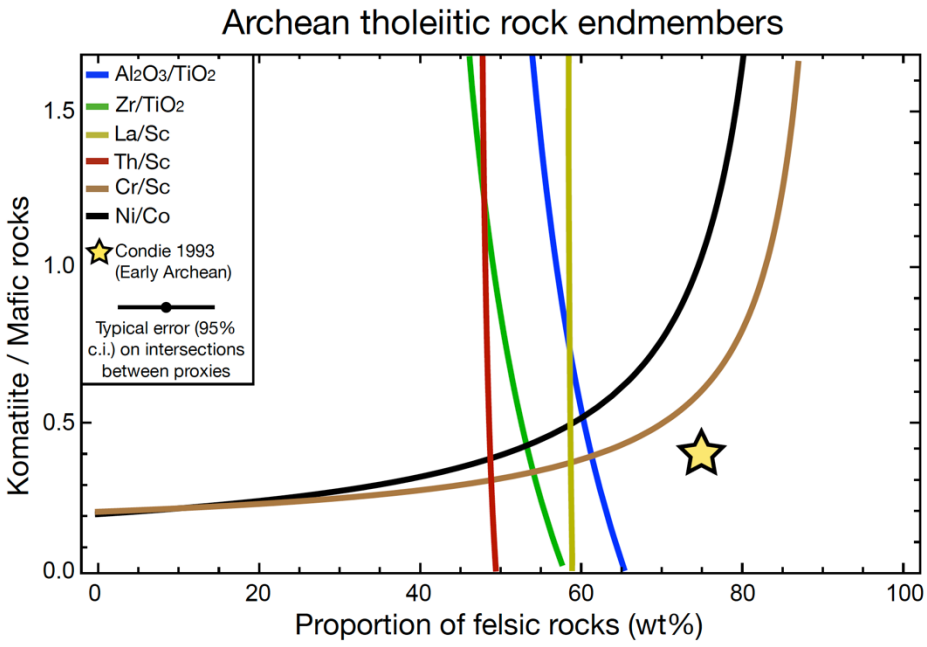

749

750 Figure S7. Test to evaluate if felsic and mafic endmembers defined by Archean tholeiitic rocks would translate
751 the 3.25 Gyr old fine-grained terrigenous sediment record into a mafic emerged crust. As shown, using these
752 endmembers leads to a bigger scatter than observed in our initial and preferred model, but would still call for
753 ~55wt% felsic rocks in the Paleoarchean emerged crust.

754

References

Adam, J. & Green, T. (2006). Trace element partitioning between mica- and amphibole-bearing garnet lherzolite and hydrous basanitic melt: 1. Experimental results and the investigation of controls on partitioning behaviour. *Contributions to Mineralogy and Petrology* **152**, 1–17.

Annen, C., Blundy, J. D. & Sparks, R. S. J. (2005). The Genesis of Intermediate and Silicic Magmas in Deep Crustal Hot Zones. *Journal of Petrology* **47**, 505–539.

Arndt, N. (2003). Komatiites, kimberlites, and boninites. *Journal of Geophysical Research Solid Earth* **108**, 2293.

Arndt, N. & Davaille, A. (2013). Episodic Earth evolution. *Tectonophysics*. Elsevier B.V. **609**, 661–674.

Barbarin, B. (1999). A review of the relationships between granitoid types, their origins and their geodynamic environments. *Lithos* **46**, 605–626.

Bindeman, I. N., Bekker, A. & Zakharov, O. D. (2016). Oxygen isotope perspective on crustal evolution on early Earth: A record of Precambrian shales with emphasis on Paleoproterozoic glaciations and Great Oxygenation Event. *Earth and Planetary Science Letters*. Elsevier B.V. **437**, 101–113.

Bindeman, I. N., Zakharov, D. O., Palandri, J., Greber, N. D., Dauphas, N., Retallack, G. J., Hofmann, A., Lackey, J. S. & Bekker, A. (2018). Rapid emergence of subaerial landmasses and onset of a modern hydrologic cycle 2.5 billion years ago. *Nature* **557**, 545–548.

Bouchez, J., Gaillardet, J., France-Lanord, C., Maurice, L. & Dutra-Maia, P. (2011). Grain size control of river suspended sediment geochemistry: Clues from Amazon River depth profiles. *Geochemistry Geophysics Geosystems* **12**.

Campbell, I. H. & Allen, C. M. (2008). Formation of supercontinents linked to increases in atmospheric oxygen. *Nature Geoscience* **1**, 554–558.

Canfield, D. E. (2005). The early history of atmospheric oxygen: homage to Robert M. Garrels. *Annual Review of Earth and Planetary Sciences* **33**, 1–36.

Cawood, P. A. & Hawkesworth, C. J. (2015). Temporal relations between mineral deposits and global tectonic cycles. *Geological Society, London, Special Publications* **393**, 9–21.

Cawood, P. A., Hawkesworth, C. J., Pisarevsky, S. A., Dhuime, B., Capitanio, F. A. & Nebel, O. (2018). Geological archive of the onset of plate tectonics. *Philosophical Transactions of the Royal Society A: Mathematical, Physical and Engineering Sciences* **376**, 20170405–30.

Condie, K. C. (1993). Chemical composition and evolution of the upper continental crust: contrasting results from surface samples and shales. *Chemical Geology* **104**, 1–37.

Condie, K. C. (2005). Earth as an evolving planetary system. Academic Press.

Condie, K. C. & O'Neill, C. (2011). The Archean-Proterozoic boundary: 500 my of tectonic transition in Earth history. *American Journal of Science* **310**, 775–790.

Condie, K. C., Arndt, N., Davaille, A. & Puetz, S. J. (2017). Zircon age peaks: Production or preservation of continental crust? *Geosphere* **13**, 227–234.

Defant, M. J. & Drummond, M. S. (1990). Derivation of Some Modern Arc Magmas by Melting of Young Subducted Lithosphere. *Nature* **347**, 662–665.

Deng, Z., Chaussidon, M., Savage, P., Robert, F., Pik, R. & Moynier, F. (2019). Titanium isotopes as a tracer for the plume or island arc affinity of felsic rocks. *Proceedings of the National Academy of Sciences of the United States of America* **116**, 1132–1135.

Dhuime, B., Wuestefeld, A. & Hawkesworth, C. J. (2015). Emergence of modern continental crust about 3 billion years ago. *Nature Geoscience* **8**, 552–555.

Doucet, S., Scoates, J. S., Weis, D. & Giret, A. (2005). Constraining the components of the Kerguelen mantle plume: A Hf-Pb-Sr-Nd isotopic study of picrites and high-MgO basalts from the Kerguelen Archipelago. *Geochemistry Geophysics Geosystems* **6**, n/a–n/a.

799 Dürr, H. H., Meybeck, M. & Dürr, S. H. (2005). Lithologic composition of the Earth's continental surfaces derived from a new
800 digital map emphasizing riverine material transfer. *Global Biogeochemical Cycles* **19**, 1–22.

801 Flament, N., Coltice, N. & Rey, P. F. (2013). The evolution of the $^{87}Sr/^{86}Sr$ of marine carbonates does not constrain continental
802 growth. *Precambrian Research*. Elsevier B.V. **229**, 177–188.

803 Foley, B. J. (2018). The dependence of planetary tectonics on mantle thermal state: applications to early Earth evolution. *Philo-*
804 *sophical Transactions of the Royal Society A: Mathematical, Physical and Engineering Sciences* **376**, 20170409–30.

805 Foley, S. F., Tiepolo, M. & Vannucci, R. (2002). Growth of early continental crust controlled by melting of amphibolite in sub-
806 duction zones. *Nature* **417**, 837–840.

807 Gale, A., Dalton, C. A., Langmuir, C. H., Su, Y., Schilling, J.-G. (2013). The mean composition of ocean ridge basalts. *Geochem-*
808 *istry Geophysics Geosystems*, **14**, 489–518.

809 Garcia, D., Coelho, J. & Perrin, M. (1991). of sorting within shale and sandstone series (northern Portugal). *European Journal of*
810 *Mineralogy* **3**, 401–414.

811 Garcia, D., Fonteilles, M. & Moutte, J. (1994). Sedimentary fractionations between Al, Ti, and Zr and the genesis of strongly per-
812 aluminous granites. *The Journal of Geology* **102**, 411–422.

813 Garçon, M., Chauvel, C. & France-Lanord, C. (2013a). Continental sedimentary processes decouple Nd and Hf isotopes. *Geochi-*
814 *mica et Cosmochimica Acta* **121**, 177–195.

815 Garçon, M., Chauvel, C., France-Lanord, C., Huyghe, P. & Lavé, J. (2013b). Continental sedimentary processes decouple Nd and
816 Hf isotopes. *Geochimica et Cosmochimica Acta*. Elsevier Ltd **121**, 177–195.

817 Garçon, M., Chauvel, C., France-Lanord, C., Limonta, M. & Garzanti, E. (2014). Which minerals control the Nd–Hf–Sr–Pb iso-
818 topic compositions of river sediments? *Chemical Geology*. Elsevier B.V. **364**, 42–55.

819 Garzanti, E., Andó, S., France-Lanord, C., Censi, P., Pietro Vignola, Galy, V. & Lupker, M. (2011). Mineralogical and chemical
820 variability of fluvial sediments 2. Suspended-load silt (Ganga–Brahmaputra, Bangladesh). *Earth and Planetary Science Let-*
821 *ters*. Elsevier B.V. **302**, 107–120.

822 Gaschnig, R. M., Rudnick, R. L., McDonough, W. F., Kaufman, A. J., Valley, J. W., Hu, Z., Gao, S. & Beck, M. L. (2016). Com-
823 positional evolution of the upper continental crust through time, as constrained by ancient glacial diamictites. *Geochimica et*
824 *Cosmochimica Acta*. Elsevier Ltd **186**, 316–343.

825 GeoRoc., <http://georoc.mpch-mainz.gwdg.de/georoc/>, accessed November 2018

826 Greber, N. D., Dauphas, N., Bekker, A., Ptáček, M. P., Bindeman, I. N. & Hofmann, A. (2017a). Titanium isotopic evidence for
827 felsic crust and plate tectonics 3.5 billion years ago. *Science* **357**, 1271–1274.

828 Greber, N. D., Dauphas, N., Puchtel, I. S., Hofmann, B. A. & Arndt, N. (2017b). Titanium stable isotopic variations in chondrites,
829 achondrites and lunar rocks. *Geochimica et Cosmochimica Acta*. Elsevier Ltd **213**, 534–552.

830 Grove, T. L., Till, C. B. & Krawczynski, M. J. (2012). The Role Zone Magmatism. *Annual Review of Earth and Planetary Sci-*
831 *ences* **40**, 413–439.

832 Hamelin C., Seitz H.-M., Barrat J.-A., Dosso L., Maury R. C. and Chaussidon M. (2009). A low δ^7Li lower crustal component:
833 Evidence from an alkalic intraplate volcanic series (Chaîne des Puys, French Massif Central). *Chemical Geology* **266**, 205–
834 217.

835 Hartmann, J. & Moosdorf, N. (2012). The new global lithological map database GLiM: A representation of rock properties at the
836 Earth surface. *Geochemistry Geophysics Geosystems* **13**, 119–37.

837 Hawkesworth, C. J. & Brown, M. (2018). Earth dynamics and the development of plate tectonics. *Philosophical Transactions of*
838 *the Royal Society A: Mathematical, Physical and Engineering Sciences* **376**, 20180228–5.

839 Hawkesworth, C., Cawood, P., Kemp, T., Storey, C. & Dhuime, B. (2009). A Matter of Preservation. *Science* **323**, 49–50.

840 Hildreth, W. & Moorbath, S. (1988). Crustal Contributions to Arc Magmatism in the Andes of Central Chile. *Contributions to*
841 *Mineralogy and Petrology* **98**, 455–489.

842 Hooper, P. R. (2000). Chemical discrimination of Columbia River basalt flows. *Geochemistry Geophysics Geosystems*, **1**,
843 doi:10.1029/2000GC000040.

Hopkins, M. D., Harrison, T. M. & Manning, C. E. (2010). Constraints on Hadean geodynamics from mineral inclusions in >4Ga zircons. *Earth and Planetary Science Letters*. Elsevier B.V. **298**, 367–376.

Jagoutz, O. & Kelemen, P. B. (2015). Role of Arc Processes in the Formation of Continental Crust. *Annual Review of Earth and Planetary Sciences* **43**, 363–404.

Jagoutz, O. E. (2010). Construction of the granitoid crust of an island arc. Part II: a quantitative petrogenetic model. *Contributions to Mineralogy and Petrology* **160**, 359–381.

Jagoutz, O. E., Burg, J. P., Hussain, S., Dawood, H., Pettke, T., Iizuka, T. & Maruyama, S. (2009). Construction of the granitoid crust of an island arc part I: geochronological and geochemical constraints from the plutonic Kohistan (NW Pakistan). *Contributions to Mineralogy and Petrology* **158**, 739–755.

Kelemen, P. B., Hanghøj, K. & Greene, A. R. (2014). 4.21 One view of the geochemistry of subduction-related magmatic arcs, with an emphasis on primitive andesite and lower crust. *Treatise on Geochemistry* 749–806.

Kelemen, P. B., Johnson, K., Kinzler, R. J. & Nature, A. I. (1990). High-field-strength element depletions in arc basalts due to mantle–magma interaction. *Nature* **345**, 521–524.

Keller, B. & Schoene, B. (2018). Plate tectonics and continental basaltic geochemistry throughout Earth history. *Earth and Planetary Science Letters*. Elsevier B.V. **481**, 290–304.

Keller, C. B. & Schoene, B. (2012). Statistical geochemistry reveals disruption in secular lithospheric evolution about 2.5 Gyr ago. *Nature*. Nature Publishing Group **485**, 490–493.

Keller, C. B., Boehnke, P. & Schoene, B. (2017). Temporal variation in relative zircon abundance throughout Earth history. *Geochemical Perspectives Letters* 179–189.

Korenaga, J. (2018). Crustal evolution and mantle dynamics through Earth history. *Philosophical Transactions of the Royal Society A: Mathematical, Physical and Engineering Sciences* **376**, 20170408–35.

Large, R. R., Mukherjee, I., Zhukova, I., Corkrey, R., Stepanov, A. & Danyushevsky, L. V. (2018). Role of upper-most crustal composition in the evolution of the Precambrian ocean–atmosphere system. *Earth and Planetary Science Letters*. Elsevier B.V. **487**, 44–53.

Le Bas, M. J. & Streckeisen, A. L. (1991). The IUGS systematics of igneous rocks. *Journal of the Geological Society* **148**, 825–833.

Lee, C.-T. A., Yeung, L. Y., McKenzie, N. R., Yokoyama, Y., Ozaki, K. & Lenardic, A. (2016). Two-step rise of atmospheric oxygen linked to the growth of continents. *Nature Geoscience*. Nature Publishing Group **9**, 1–10.

Lenardic, A. (2018). The diversity of tectonic modes and thoughts about transitions between them. *Philosophical Transactions of the Royal Society A: Mathematical, Physical and Engineering Sciences* **376**, 20170416–22.

Li X., Li J., Bader T., Mo X., Scheltens M., Chen Z., Xu J., Yu X. and Huang X. (2015). Evidence for crustal contamination in intra-continental OIB-like basalts from West Qinling, central China: A Re–Os perspective. *Journal of Asian Earth Sciences* **98**, 436–445.

Lupker, M., France-Lanord, C., Lavé, J., Bouchez, J., Galy, V., Métivier, F., Gaillardet, J., Lartiges, B. & Mugnier, J.-L. (2011). A Rouse-based method to integrate the chemical composition of river sediments: Application to the Ganga basin. *Geophysical Research Letters* **116**, 488–24.

Lyons, T. W., Reinhard, C. T. & Planavsky, N. J. (2014). The rise of oxygen in Earth's early ocean and atmosphere. *Nature* **506**, 307–315.

McLennan, S. M., Hemming, S., McDaniel, D. K. & Hanson, G. N. (1993). Geochemical approaches to sedimentation, provenance, and tectonics. *Geological Society of America Special Paper 284*, 21–40.

MacDonald, G.A., Katsura, T. (1964). Chemical Composition of Hawaiian Lavas, *Journal of Petrology* **5**, 82–133.

Millet, M.-A. & Dauphas, N. (2014). Ultra-precise titanium stable isotope measurements by double-spike high resolution MC-ICP-MS. *Journal of Analytical Atomic Spectrometry* **29**, 1444.

Millet, M.-A., Dauphas, N., Greber, N. D., Burton, K. W., Dale, C. W., Debret, B., Macpherson, C. G., Nowell, G. M. & Williams, H. M. (2016). Titanium stable isotope investigation of magmatic processes on the Earth and Moon. *Earth and Planetary Science Letters*. Elsevier B.V. **449**, 197–205.

Moosdorf, N., Hartmann, J. & Dürr, H. H. (2010). Lithological composition of the North American continent and implications of lithological map resolution for dissolved silica flux modeling. *Geochemistry Geophysics Geosystems* **11**, n/a–n/a.

Moyen, J.-F. & Laurent, O. (2018). Archaean tectonic systems: A view from igneous rocks. *Lithos*. Elsevier B.V. **302-303**, 99–125.

Moyen, J.-F. & Martin, H. (2012). Forty years of TTG research. *Lithos*. Elsevier B.V. **148**, 312–336.

Münker, C., Wörner, G., Yogodzinski, G. & Churikova, T. (2004). Behaviour of high field strength elements in subduction zones: constraints from Kamchatka–Aleutian arc lavas. *Earth and Planetary Science Letters* **224**, 275–293.

Müntener, O. & Ulmer, P. (2018). Arc crust formation and differentiation constrained by experimental petrology. *American Journal of Science* **318**, 64–89.

Miyashiro, A. (1974). Volcanic Rock Series in Island Arcs and Active Continental Margins, *American Journal of Science*. **274**, 321–355.

PetDB., < https://www.earthchem.org/petdb>, accessed November 2018

Polat, A., Wang, L. & Appel, P. W. U. (2015). A review of structural patterns and melting processes in the Archean craton of West Greenland: Evidence for crustal growth at convergent plate margins as opposed to non-uniformitarian models. *Tectonophysics*. Elsevier B.V. **662**, 67–94.

Powell, D. M. (1998). Patterns and processes of sediment sorting in gravel-bed rivers. *Progress in Physical Geography* **22**, 1–32.

Prytulak, J. & Elliott, T. (2007). TiO2 enrichment in ocean island basalts. *Earth and Planetary Science Letters* **263**, 388–403.

Reimink, J. R., Chacko, T., Carlson, R. W., Shirey, S. B., Liu, J., Stern, R. A., Bauer, A. M., Pearson, D. G. & Heaman, L. M. (2018). Petrogenesis and tectonics of the Acasta Gneiss Complex derived from integrated petrology and 142Nd and 182W extinct nuclide-geochemistry. *Earth and Planetary Science Letters*. Elsevier B.V. **494**, 12–22.

Rey, P. F. & Coltice, N. (2008). Neoarchean lithospheric strengthening and the coupling of Earth's geochemical reservoirs. *Geology* **36**, 635–638.

Roberts, N. M. W. & Spencer, C. J. (2015). The zircon archive of continent formation through time. *Geological Society, London, Special Publications* **389**, 197–225.

Rudnick, R. L. & Gao, S. X. (2003). Composition of the continental crust. *Treatise on Geochemistry* pp. 659.

Sizova, E., Gerya, T., Stüwe, K. & Brown, M. (2015). Generation of felsic crust in the Archean: A geodynamic modeling perspective. *Precambrian Research*. Elsevier B.V. **271**, 198–224.

Smart, K. A., Tappe, S., Stern, R. A., Webb, S. J. & Ashwal, L. D. (2016). Early Archaean tectonics and mantle redox recorded in Witwatersrand diamonds. *Nature Geoscience* **9**, 255–259.

Smit, M. A. & Mezger, K. (2017). Earth's early O_2 cycle suppressed by primitive continents. *Nature Geoscience* **10**, 788–792.

Tang, M., Chen, K. & Rudnick, R. L. (2016). Archean upper crust transition from mafic to felsic marks the onset of plate tectonics. *Science* **351**, 372–375.

Taylor, S. R. & McLennan, S. M. (1985). *The continental crust: its composition and evolution*. Oxford: Blackwell Scientific.

Ulmer, P. (2001). Partial melting in the mantle wedge - the role of genesis of mantle-derived "arc-related" magmas. *Physics of the Earth and Planetary Interiors* **127**, 215–232.

Van Kranendonk, M. J., Smithies, R. H., Griffin, W. L., Huston, D. L., Hickman, A. H., Champion, D. C., Anhaeusser, C. R. & Pirajno, F. (2015). Making it thick: a volcanic plateau origin of Palaeoarchean continental lithosphere of the Pilbara and Kaapvaal cratons. *Geological Society, London, Special Publications* **389**, 83–111.

Vanderkluysen, L., Mahoney, J. J., Hooper, P. R., Sheth, H. C. & Ray, R. (2011). The Feeder System of the Deccan Traps (India): Insights from Dike Geochemistry. *Journal of Petrology* **52**, 315–343.

Voice, P. J., Kowalewski, M. & Eriksson, K. A. (2011). Quantifying the Timing and Rate of Crustal Evolution: Global Compilation of Radiometrically Dated Detrital Zircon Grains. *The Journal of Geology* **119**, 109–126.

Wedepohl, H. K. (1995). The composition of the continental crust. *Geochimica et Cosmochimica Acta* **59**, 1217–1232.

Woodhead, J. D., Eggins, S. M. & Johnson, R. W. (1998). Magma genesis in the New Britain island arc: Further insights into melting and mass transfer processes. *Journal of Petrology* **39**, 1641–1668.

Worsley, T. R., Nance, D., Moody, J. B.1984 (1984). Global tectonics and eustasy for the past 2 billion years. *Marine Geology* **58**, 373–400.

References used for data compilation (Table S1):

Absar, Nurul, Mahshar Raza, Minati Roy, S. M. Naqvi, and Ashim K. Roy. 2009. "Composition and Weathering Conditions of Paleoproterozoic Upper Crust of Bundelkhand Craton, Central India: Records from Geochemistry of Clastic Sediments of 1.9 Ga Gwalior Group." Precambrian Research 168 (3–4): 313–29.

Armstrong-Altrin, J. S., Nagarajan, R., Madhavaraju, J., Rosalez-Hoz, L., Lee, Il, Y., Balaram, V., et al. (2013). Geochemistry of the Jurassic and Upper Cretaceous shales from the Molango Region, Hidalgo, eastern Mexico: Implications for source-area weathering, provenance, and tectonic setting. Comptes Rendus-Géoscience, 345(4), 185–202.

Armstrong-Altrin, J. S., & Machain-Castillo, M. L. (2016). Mineralogy, geochemistry, and radiocarbon ages of deep sea sediments from the Gulf of Mexico, Mexico. Journal of South American Earth Sciences, 71, 182-200.

Bangert, B. (2000). Tephrostratigraphy, petrography, geochemistry, age and fossil record of the Ganigobis Shale Member and associated glaciomarine deposits of the Dwyka Group, Late Carboniferous, southern Africa. PhD Dissertation. Bayerischen Julius-Maximilians-Universität Würzburg. p. 243.

Bindeman, I. N., Bekker, A., and Zakharov, D. O. 2016. "Oxygen Isotope Perspective on Crustal Evolution on Early Earth: A Record of Precambrian Shales with Emphasis on Paleoproterozoic Glaciations and Great Oxygenation Event." Earth and Planetary Science Letters 437 (March): 101–13. doi:10.1016/j.epsl.2015.12.029.

Bhat, M. I, and S. K Ghosh. 2001. "Geochemistry of the 2.51 Ga Old Rampur Group Pelites, Western Himalayas: Implications for Their Provenance and Weathering." Precambrian Research 108 (1–2): 1–16. doi:10.1016/S0301-9268(00)00139-X.

Bolhar, R., Hofmann, A., Siahi, M., Feng, Y.-X., & Delvigne, C. (2015). A trace element and Pb isotopic investigation into the provenance and deposition of stromatolitic carbonates, ironstones and associated shales of the ~3.0 Ga Pongola Supergroup, Kaapvaal Craton. Geochimica et Cosmochimica Acta, 158(C), 57–78.

Böttcher, M. E., Rinna, J., Warning, B., Wehausen, R., Howell, M. W., Schnetger, B., Stein, R., Brumsack, H.J., Rullkötter, J. (2003). Geochemistry of sediments from the connection between the western and the eastern Mediterranean Sea (Strait of Sicily, ODP Site 963). Palaeogeography, Palaeoclimatology, Palaeoecology, 190, 165-194.

Boudec, A. L., Ineson, J., Rosing, M., Døssing, L., Martineau, F., Lécuyer, C., & Albarède, F. (2014). Geochemistry of the Cambrian Sirius Passet Lagerstätte, Northern Greenland. Geochemistry Geophysics Geosystems, 15(4), 886–904.

Cabral, A. R., Creaser, R. A., Nägler, T., Lehmann, B., Voegelin, A. R., Belyatsky, B., et al. (2013). Trace-element and multi-isotope geochemistry of Late-Archean black shales in the Carajás iron-ore district, Brazil. Chemical Geology, 362(C), 91–104.

Campos Alvarez, N., & Roser, B. P. (2007). Geochemistry of black shales from the Lower Cretaceous Paja Formation, Eastern Cordillera, Colombia: Source weathering, provenance, and tectonic setting. Journal of South American Earth Sciences, 23(4), 271–289.

Caplan, M. L., & Bustin, R. M. (1998). Palaeoceanographic controls on geochemical characteristics of organic-rich Exshaw mudrocks: role of enhanced primary production. Organic Geochemistry, 30, 161–188.

Carmichael, S. K., Waters, J. A., Batchelor, C. J., Coleman, D. M., Suttner, T. J., Kido, E., et al. (2015). Climate instability and tipping points in the Late Devonian: Detection of the Hangenberg Event in an open oceanic island arc in the Central Asian Orogenic Belt. Gondwana Research, 1–19.

Condie, Kent C, Dennis Lee, and G. Lang Farmer. 2001. "Tectonic Setting and Provenance of the Neoproterozoic Uinta Mountain and Big Cottonwood Groups, Northern Utah: Constraints from Geochemistry, Nd Isotopes, and Detrital Modes." Sedimentary Geology 141–142 (June): 443–64. doi:10.1016/S0037-0738(01)00086-0.

Cullers, Robert L, and Victor N Podkovyrov. 2000. "Geochemistry of the Mesoproterozoic Lakhanda Shales in Southeastern Yakutia, Russia: Implications for Mineralogical and Provenance Control, and Recycling." Precambrian Research 104 (1–2): 77–93. doi:10.1016/S0301-9268(00)00090-5.

Deru, Xu, Gu Xuexiang, Li Pengchun, Chen Guanghao, Xia Bin, Robert Bachlinski, He Zhuanli, and Fu Gonggu. 2007. "Mesoproterozoic–Neoproterozoic Transition: Geochemistry, Provenance and Tectonic Setting of Clastic Sedimentary Rocks on the SE Margin of the Yangtze Block, South China." Journal of Asian Earth Sciences 29 (5–6): 637–50. doi:10.1016/j.jseaes.2006.04.006.

Devaraju, T. C., T. L. Sudhakara, R. J. Kaukonen, R. P. Viljoen, T. T. Alapieti, S. A. Ahmed, and S. Sivakumar. 2010. "Petrology and Geochemistry of Greywackes from Goa-Dharwar Sector, Western Dharwar Craton: Implications for Volcanoclastic Origin." Journal of the Geological Society of India 75 (3): 465–87. doi:10.1007/s12594-010-0050-8.

Dypvik, H., & Zakharov, V. (2012). Fine-grained epicontinental Arctic sedimentation – mineralogy and geochemistry of shales from the Late Jurassic-Early Cretaceous transition. Norwegian Journal of Geology, 92, 65–87.

Eriksson, K. A., Taylor, S. R. and Korsch, R. J. 1992. "Geochemistry of 1.8-1.67 Ga Mudstones and Siltstones from the Mount Isa Inlier, Queensland Australia: Provenance and Tectonic Implications." Geochimica et Cosmochimica Acta 56 (3): 899–909. doi:10.1016/0016-7037(92)90035-H.

Fedo, Christopher M., Kenneth A. Eriksson, and Eirik J. Krogstad. 1996. "Geochemistry of Shales from the Archean (~3.0 Ga) Buhwa Greenstone Belt, Zimbabwe: Implications for Provenance and Source-Area Weathering." Geochimica et Cosmochimica Acta 60 (10): 1751–63. doi:10.1016/0016-7037(96)00058-0.

Feng, R., and R. Kerrich. 1990. "Geochemistry of Fine-Grained Clastic Sediments in the Archean Abitibi Greenstone Belt, Canada: Implications for Provenance and Tectonic Setting." Geochimica et Cosmochimica Acta 54 (4): 1061–81. doi:10.1016/0016-7037(90)90439-R.

Fu, X., Tan, F., Feng, X., Wang, D., Chen, W., Song, C., & Zeng, S. (2014). Early Jurassic anoxic conditions and organic accumulation in the eastern Tethys. International Geology Review, 56(12), 1450–1465.

Gaschnig, R. M., Rudnick, R. L., McDonough, W. F., Kaufman, A. J., Valley, J. W., Hu, Z., Gao, S., & Beck, M. L. (2016). Compositional evolution of the upper continental crust through time, as constrained by ancient glacial diamictites. Geochimica et Cosmochimica Acta, 186, 316-343. (Supplementary data 2)

Gibbs, Allan K., Carla W. Montgomery, Peggy A. O'Day, and Eric A. Erslev. 1986. "The Archean-Proterozoic Transition: Evidence from the Geochemistry of Metasedimentary Rocks of Guyana and Montana." Geochimica et Cosmochimica Acta 50 (10): 2125–41. doi:10.1016/0016-7037(86)90067-0.

Hayashi, Ken-Ichiro, Hiroyuki Fujisawa, Heinrich D. Holland, and Hiroshi Ohmoto. 1997. "Geochemistry of ~1.9 Ga Sedimentary Rocks from Northeastern Labrador, Canada." Geochimica et Cosmochimica Acta 61 (19): 4115–37. doi:10.1016/S0016-7037(97)00214-7.

Hegde, V. S., and V. C. Chavadi. 2009. "Geochemistry of Late Archaean Metagreywackes from the Western Dharwar Craton, South India: Implications for Provenance and Nature of the Late Archaean Crust." Gondwana Research 15 (2): 178–87. doi:10.1016/j.gr.2008.09.006.

Hetzel, A., Böttcher, M. E., Wortmann, U. G., & Brumsack, H.-J. J. (2009). Paleo-redox conditions during OAE 2 reflected in Demerara Rise sediment geochemistry (ODP Leg 207). Palaeogeography, Palaeoclimatology, Palaeoecology, 273(3-4), 302–328.

Hofmann, Axel. 2005. "The Geochemistry of Sedimentary Rocks from the Fig Tree Group, Barberton Greenstone Belt: Implications for Tectonic, Hydrothermal and Surface Processes during Mid-Archaean Times." Precambrian Research 143 (1–4): 23–49. doi:10.1016/j.precamres.2005.09.005.

Hofmann, Axel, Robert Bolhar, Paul Dirks, and Hielke Jelsma. 2003. "The Geochemistry of Archaean Shales Derived from a Mafic Volcanic Sequence, Belingwe Greenstone Belt, Zimbabwe: Provenance, Source Area Unroofing and Submarine versus Subaerial Weathering." Geochimica et Cosmochimica Acta 67 (3): 421–40. doi:10.1016/S0016-7037(02)01086-4.

Huang, J., Chu, X., Lyons, T. W., Planavsky, N. J., & Wen, H. (2013). A new look at saponite formation and its implications for early animal records in the Ediacaran of South China. Geobiology, 11(1), 3–14.

Hu, D., Böning, P., Köhler, C. M., Hillier, S., Pressling, N., Wan, S., Brumsack, H.J., Clift, P. D. (2012). Deep sea records of the continental weathering and erosion response to East Asian monsoon intensification since 14ka in the South China Sea. Chemical Geology, 326, 1-18.

Hu and Gao (2008), Upper crustal abundances of trace elements: A revision and update, Chemical Geology 253, pp 205-211

Lézin, C., Andreu, B., Pellenard, P., Bouchez, J.-L., Emmanuel, L., Fauré, P., & Landrein, P. (2013). Geochemical disturbance and paleoenvironmental changes during the Early Toarcian in NW Europe. Chemical Geology, 341(C), 1–15.

1029 Lobach-Zhuchenko, S. B., V. V. Balagansky, Sh K. Baltybaev, G. V. Artemenko, E. S. Bogomolov, A. V. Yurchenko, L. M. Ste-
1030 panyuk, and V. V. Sukach. 2014. "Metasedimentary Rocks of the Paleoarchean Dniester-Bug Group, Ukrainian Shield: Com-
1031 position, Age, and Sources." Lithology and Mineral Resources 49 (5): 381–97. doi:10.1134/S002449021405006X.

1032 Manikyamba, C., and R. Kerrich. 2006. "Geochemistry of Black Shales from the Neoarchaean Sandur Superterrane, India: First
1033 Cycle Volcanogenic Sedimentary Rocks in an Intraoceanic Arc–trench Complex." Geochimica et Cosmochimica Acta 70
1034 (18): 4663–79. doi:10.1016/j.gca.2006.07.015.

1035 Manikyamba, C., Kerrich, R., González-Álvarez, I., Mathur, R., & Khanna, T. C. (2008). Geochemistry of Paleoproterozoic black
1036 shales from the Intracontinental Cuddapah basin, India: implications for provenance, tectonic setting, and weathering inten-
1037 sity. Precambrian Research, 162(3-4), 424–440.

1038 Marynowski, L., Zatoń, M., Rakociński, M., Filipiak, P., Kurkiewicz, S., & Pearce, T. J. (2012). Deciphering the upper
1039 Famennian Hangenberg Black Shale depositional environments based on multi-proxy record. Palaeogeography, Palaeoclima-
1040 tology, Palaeoecology, 346-347, 66–86.

1041 Maslov, A. V., Isherskaya, M. V., Ronkin, Yu. L., Krupenin, M. T., Gorbunova, N. P., Gulyaeva, T. Ya., Lepikhina, O. P.,
1042 Popova, O. Yu., Yatluk, G. M., (2006). Mudstone lithogeochemistry and formation conditions of Vendian deposits in the
1043 Shkapovo-Shikhan Basin. Lithology and Mineral Resources 41.3, 250-270.

1044 McLennan, S. M., Taylor, S. R., and Kröner, A. 1983. "Geochemical Evolution of Archean Shales from South Africa. I. The Swa-
1045 ziland and Pongola Supergroups." Precambrian Research 22 (1): 93–124. doi:10.1016/0301-9268(83)90060-8.

1046 McLennan, Scott M, Taylor, S. R., and McGregor, V. R. 1984. "Geochemistry of Archean Metasedimentary Rocks from West
1047 Greenland." Geochimica et Cosmochimica Acta 48 (1): 1–13. doi:10.1016/0016-7037(84)90345-4.

1048 McLennan, Scott M., Taylor, S. R., and Eriksson, K. A. 1983. "Geochemistry of Archean Shales from the Pilbara Supergroup,
1049 Western Australia." Geochimica et Cosmochimica Acta 47 (7): 1211–22. doi:10.1016/0016-7037(83)90063-7.

1050 McLennan, S. M., Hemming, S. R., Taylor, S. R., and Eriksson, K. A. 1995. "Early Proterozoic Crustal Evolution: Geochemical
1051 and NdPb Isotopic Evidence from Metasedimentary Rocks, Southwestern North America." Geochimica et Cosmochimica
1052 Acta 59 (6): 1153–77. doi:10.1016/0016-7037(95)00032-U.

1053 Nagarajan, R., Madhavaraju, J., & Nagendra, R. (2007). Geochemistry of Neoproterozoic shales of the Rabanpalli Formation,
1054 Bhima Basin, Northern Karnataka, southern India: implications for provenance and paleoredox conditions. Revisa Mexicana
1055 De Ciencias Geológicas, 24, 150–160.

1056 Perkins, R. B., Piper, D. Z., & Mason, C. E. (2008). Trace-element budgets in the Ohio/Sunbury shales of Kentucky: Constraints
1057 on ocean circulation and primary productivity in the Devonian–Mississippian Appalachian Basin. Palaeogeography, Palaeo-
1058 climatology, Palaeoecology, 265, 14–29.

1059 Plank, T., & Langmuir, C. H. (1998). The chemical composition of subducting sediment and its consequences for the crust and
1060 mantle. Chemical geology, 145(3), 325-394. Table 1

1061 Prame, W. K. B. N., and Pohl, J. 1994. "Geochemistry of Pelitic and Psammopelitic Precambrian Metasediments from Southwest-
1062 ern Sri Lanka: Implications for Two Contrasting Source-Terrains and Tectonic Settings." Precambrian Research 66 (1): 223–
1063 44. doi:10.1016/0301-9268(94)90052-3.

1064 Porebska, E., & Sawlowicz, Z. (1997). Palaeoceanographic linkage of geochemical and graptolite events across the Silurian-De-
1065 vonian boundary in Bardzkie Mountians (Southwest Poland). Palaeogeography, Palaeoclimatology, Palaeoecology, 132, 343–
1066 354.

1067 Racka, M., Marynowski, L., Filipiak, P., Sobstel, M., Pisarzowska, A., & Bond, D. P. G. (2010). Anoxic Annulata Events in the
1068 Late Famennian of the Holy Cross Mountains (Southern Poland): Geochemical and palaeontological record. Palaeogeogra-
1069 phy, Palaeoclimatology, Palaeoecology, 297(3-4), 549–575.

1070 Rao, V., Sreenivas, B., Balaram, V., & Govil, P. K. (1999). The nature of the Archean upper crust as revealed by the geochemis-
1071 try of the Proterozoic shales of the Kaladgi basin, Karnataka, southern India. Precambrian Research, 98(1-2), 53–65.

1072 Raza, M., Ahmad, A.H.M., Khan, M.S., Khan, F. 2012. Geochemistry and detrital modes of Proterozoic sedimentary rocks, Ba-
1073 yana Basin, north Delhi fold belt: implications for provenance and source-area weathering. International Geology Review, 54,
1074 111-129.

1075 Sensarma, S., Chakraborty, P., Banerjee, R., & Mukhopadhyay, S. (2016). Geochemical fractionation of Ni, Cu and Pb in the
1076 deep sea sediments from the Central Indian Ocean Basin: An insight into the mechanism of metal enrichment in sediment.
1077 Chemie der Erde-Geochemistry, 76(1), 39-48.

Sun, W.-H., Zhou, M.-F., Yan, D.-P., Li, J.-W., Ma, Y.-X., (2008), Provenance and tectonic setting of the Neoproterozoic Yanbian Group, western Yangtze Block (SW China). Precambrian Research 167.1, 213-236.

Turner, E. C., & Kamber, B. S. (2012). Arctic Bay Formation, Borden Basin, Nunavut (Canada): Basin evolution, black shale, and dissolved metal systematics in the Mesoproterozoic ocean. Precambrian Research, 208-211, 1–18.

Wille, Martin, Oliver Nebel, Martin J. Van Kranendonk, Ronny Schoenberg, Ilka C. Kleinhanns, and Michael J. Ellwood. 2013. "Mo–Cr Isotope Evidence for a Reducing Archean Atmosphere in 3.46–2.76 Ga Black Shales from the Pilbara, Western Australia." Chemical Geology 340 (February): 68–76. doi:10.1016/j.chemgeo.2012.12.018.

Wani, H., and M. E. A. Mondal. 2010. "Petrological and Geochemical Evidence of the Paleoproterozoic and the Meso-Neoproterozoic Sedimentary Rocks of the Bastar Craton, Indian Peninsula: Implications on Paleoweathering and Proterozoic Crustal Evolution." Journal of Asian Earth Sciences 38 (5): 220–32. doi:10.1016/j.jseaes.2010.01.003.

Wani, H., & Mondal, M. E. A. (2011). Evaluation of provenance, tectonic setting, and paleoredox conditions of the Mesoproterozoic-Neoproterozoic basins of the Bastar craton, Central Indian Shield: Using petrography of sandstones and geochemistry of shales. Lithosphere, 3(2), 143–154.

Werne, J. P., Sageman, B. B., Lyons, T. W., & Hollander, D. J. (2002). An integrated assessment of a" type euxinic" deposit: Evidence for multiple controls on black shale deposition in the Middle Devonian Oatka Creek Formation. Proceedings of the Ocean Drilling Program, Scientific Results, 302, 110–143.

Wronkiewicz, David J., and Condie, Kent C. 1990. "Geochemistry and Mineralogy of Sediments from the Ventersdorp and Transvaal Supergroups, South Africa: Cratonic Evolution during the Early Proterozoic." Geochimica et Cosmochimica Acta 54 (2): 343–54. doi:10.1016/0016-7037(90)90323-D.

Wronkiewicz, David J., and Condie, Kent C. 1989. "Geochemistry and Provenance of Sediments from the Pongola Supergroup, South Africa: Evidence for a 3.0-Ga-Old Continental Craton." Geochimica et Cosmochimica Acta 53 (7): 1537–49. doi:10.1016/0016-7037(89)90236-6.

Wronkiewicz, David J., and Kent C. Condie. 1987. "Geochemistry of Archean Shales from the Witwatersrand Supergroup, South Africa: Source-Area Weathering and Provenance." Geochimica et Cosmochimica Acta 51 (9): 2401–16. doi:10.1016/0016-7037(87)90293-6.

Yu, B., Dong, H., Widom, E., Chen, J., & Lin, C. (2009). Geochemistry of basal Cambrian black shales and cherts from the Northern Tarim Basin, Northwest China: Implications for depositional setting and tectonic history. Journal of Asian Earth Sciences, 34(3), 418–436.

Zhou, L., Friis, H., & Poulsen, M. L. K. (2015). Geochemical evaluation of the Late Paleocene and Early Eocene shales in Siri Canyon, Danish-Norwegian Basin. Marine and Petroleum Geology, 61(C), 111–122.

Zhou, L., and Kyte., F.T., (1992), Sedimentation history of the South Pacific Pelagic Clay Province over the last 85 million years inferred from the geochemistry of deep sea drilling project Hole 596, Paleoceanography, Vol.7, No.4, pp. 441-465